Cyclonic activity in the eastern Gulf of Mexico: Characterization from along-track altimetry and in situ drifter trajectories

Matthieu Le Hénaff, Vassiliki H. Kourafalou, Renaud Dussurget, Rick Lumpkin

Cyclonic activity in the eastern Gulf of Mexico: characterization from along-track altimetry and *in situ* drifter trajectories

Matthieu Le Hénaff[1,2]

Vassiliki H. Kourafalou[1]

Renaud Dussurget[3,4]

Rick Lumpkin[5]

[1]Rosenstiel School of Marine and Atmospheric Science (RSMAS), 4600 Rickenbacker Causeway, Miami, FL 33149-1098, USA

[2]Cooperative Institute for Marine and Atmospheric Studies (CIMAS), 4600 Rickenbacker Causeway, Miami, FL 33149-1098, USA

[3]Laboratoire Environnement Resources Provence Azur Corse, Z.P. de Bregaillon, BP 330, 83507 La-Seyne-sur-Mer Cedex, France

[4]Now at Collecte Localisation Satellites, 8-10, rue Hermès, Parc Technologique du Canal, 31520 Ramonville Saint-Agne, France.

[5]NOAA Atlantic Oceanographic and Meteorological Laboratory (AOML), 4301 Rickenbacker Causeway, Miami, FL 33149, USA

Contact author:

Matthieu Le Hénaff

RSMAS/CIMAS

4600 Rickenbacker Causeway, Miami FL 33149-1098, USA

Tel: (1) 305 421 4154

Fax: (1) 305 421 4696

mlehenaff@rsmas.miami.edu

Key words

Gulf of Mexico; satellite altimetry; ocean surface drifters; cyclonic eddies; relative vorticity.

Abstract

The shedding sequence of the Loop Current (LC) inside the Gulf of Mexico (GoM) is strongly influenced by cyclonic frontal eddies around its edge. Along-track altimetry data, analyzed based on a wavelet decomposition to provide estimates of individual cyclones' diameter, amplitude and relative vorticity, and *in situ* surface drifter data from the Global Drifter Program, are used to investigate the cyclonic activity in the eastern Gulf of Mexico, where the LC extends and retracts. By analyzing this ~20 year long (1992-2011) combined set of observation data records, we were able to complement previous findings, to confirm results from modeling studies and to provide new insights on the LC frontal dynamics.

Drifter data indicate, for the first time, that Loop Current Frontal Eddies (LCFEs) are in solid-body rotation close to their core. This property makes relative vorticity the most robust diagnostic from along-track altimetry for characterizing LCFEs in the eastern GoM, based on consistent comparisons with drifter data. Both data sets are complementary for describing the LCFEs' regional variability.

LCFEs observed in the deep southeastern GoM show intense relative vorticity, but they are not frequently observed. The study of an unprecedented, long drifter trajectory suggests that

they are not intensified locally. This implies that, among LCFEs coming from the northern GoM, only intense ones reach the deep southeastern GoM.

The observation datasets provide, for the first time, quantitative evidences of processes so far only identified with models: LCFEs are intensified when they are advected over the Mississippi Fan in the northern GoM; a small area north of Campeche Bank shows intense LCFE activity.

The altimetry and drifter data confirm and complement results from more limited datasets: LCFEs forming the Tortugas Eddies, at the entrance of the Straits of Florida, are the most intensely observed LCFEs in altimetry. Coming from the GoM interior, they can be modified, in size and intensity, just before or during their stay in the Dry Tortugas area, whereas they were long considered to be modified only after they were advected in the Straits of Florida. A single drifter trajectory illustrates in detail the erosion of a LCFE in the southeastern GoM, presumably under the influence of the LC, which leads to the re-arrangement of vorticity and the formation of a distinct LCFE, just upstream the Dry Tortugas area.

The study also confirms that LCFEs have diameters of 80 to 120 km, generally larger east and north of the LC. They tend to stay for long periods in the northeastern GoM, and thus may undergo vortex merging with incoming eddies, as previously noted on individual episodes. Altimetry reveals that the largest LCFEs reside in the central eastern GoM, in a location where they are known to block the LC extension; however, our long altimetry dataset shows that these large eddies are not always involved in such LC blocking.

Finally, this study led to improvements in data treatment, for both along-track altimetry and drifter trajectories. The wavelet approach used to derive eddy characteristics from along-

track altimetry allows robust estimates of the eddy relative vorticity. The drifter dataset has been extended to include data from drifters even after they lost their drogue; the latter data treatment can be applied in areas of moderate winds.

1. Introduction

The Loop Current (LC) is the intense current that flows within the Gulf of Mexico (GoM), from the Yucatan Channel to the Straits of Florida. There, it becomes the Florida Current, before reaching the Atlantic Ocean where it becomes the Gulf Stream. As such, it is a component of the Atlantic western boundary current system. This intense flow is the dominant dynamical signal inside the GoM, and is crucial for many processes such as: biological connectivity from the Caribbean Sea to the GoM interior and toward the Atlantic (Tester et al., 1991; Lee and Williams, 1991; Paris et al., 2005); pollutant transport, as seen during the Deepwater Horizon oil spill (Walker et al., 2011, Le Hénaff et al., 2012a); and management of the numerous oil platforms of the GoM.

The LC is characterized by its variable extension inside the GoM, from a retracted position in which it flows directly from the Yucatan Channel to the Straits of Florida, also called the port-to-port situation, to an extended position in which the LC flows northward, before turning clockwise toward the GoM exit to the southeast. During the extended stage, the LC is able to reach the continental shelf break of the northern GoM, southeast of the Mississippi Delta. Then, it eventually closes its anticyclonic rotation and forms a large, warm core eddy, called a LC Eddy (LCE) or Ring. This stage often involves the transitory re-attachment of the LCE to the LC, and sometimes several temporary detachments, before the final separation of the LCE. This whole sequence is referred to as LCE shedding, and leads to sudden changes in the latitudinal extension of the LC. Once formed, the LCE then drifts westward inside the central and western GoM. During this drift, the LCE decays, and it finally breaks apart when it reaches the

continental shelf. These different stages of the LC extension are presented on Figure 1, together with the GoM bathymetry.

The LC and its variability were first described using ship survey observations (Ichye, 1962). Such *in-situ* data also revealed the presence of cold, cyclonic eddies at the edge of the LC (Cochrane, 1972). These eddies were suspected to play a role in the LCE detachment sequence. Based on 4 years of remotely sensed maps of Sea Surface Temperature (SST) and *in situ* observations from cruises, Vukovich and Maul (1985) found that these frontal cyclonic eddies east of the extended LC were usually involved in LCE shedding sequences. These cyclones were found to have 80 to 120 km diameters, maximum surface currents of about 100 cm s^{-1} and reached at least 1000 m depth (Vukovich and Maul, 1985). Vukovich (1988) did a more systematic study of the LC system, using satellite SST maps from the Advanced Very High Resolution Radiometer (AVHRR) instrument, measured over a 5-year period. He found that the cold LC perturbations associated with frontal cyclones are larger at the eastern side of the LC than at the western side, and suggested that such perturbations form or intensify northwest of the extended LC. Fratantoni et al. (1998) also used AVHRR SST maps to describe LC frontal dynamics, based on 3 years of satellite observations. They found that cyclonic eddies at the edge of the LC (LC frontal eddies, LCFEs), take part in the formation of a quasi-stationary cyclone southeast of the GoM (called "Tortugas Eddy") at the entrance of the Straits of Florida near the Dry Tortugas islands. Based on *in situ* observations in the Straits of Florida, Fratantoni et al. (1998) further suggested that the Tortugas Eddy becomes deformed and shrinks when it enters the Straits of Florida. Kourafalou and Kang (2012) found that the changes experienced by the frontal cyclones within the Straits of Florida can be due to local cyclone formation, eddy merging

or splitting, and stressed the role of the topography on eddy-eddy or eddy-mean current interactions.

Remotely sensed SST maps, as used by Vukovich and Maul (1985), Vukovich (1988) or Fratantoni et al. (1998), are of limited value in summer, when the surface waters of the GoM are almost uniformly warm and the LC signature cannot be isolated from its surroundings. Such a limitation does not affect altimetry data, which have allowed continuous measurements of Sea Level Anomaly (SLA) since the October 1992 launch of Topex/Poseidon. Although radar altimetry so far only detects SLA at the satellite nadir, such data are usually interpolated to derive gridded Sea Surface Height (SSH) maps. These maps allow the detection and characterization of the ocean's largest and most intense dynamical structures, especially currents and meso-scale eddies (Le Traon and Morrow, 2001, Morrow and Le Traon, 2011). Leben (2005) used such SLA maps to derive robust statistics about the interval between two successive LCE separations, called the separation period; he determined that this period has peaks at 6, 9 and 11.5 months, and varies between 0.5 and 18.5 months. Episodes of long separation periods coincide with the presence, in the early stage of the LC, of a large cyclone north of the LC in the port-to-port stage. This cyclone blocks the extension of the LC (Zavala-Hidalgo et al., 2002). Based on a model simulation, Zavala-Hidalgo et al. (2006) found that such a situation leads to a mass leakage from the retracted LC, which either feeds the cyclone or leads to the formation of small anticyclones along the West Florida Shelf. Zavala-Hidalgo et al. (2003) also used along-track altimetry data to study the evolution of LCFEs west of the LC along the Campeche Bank (CB). They found that these CB related LCFEs could also play a role in the shedding of a LCE. Athié et al. (2012), based on *in situ* moorings and mapped altimetry, found that these LCFEs along the CB were partly fed by cyclones advected from south of the Yucatan Channel. Using altimetry SSH maps

from Leben (2005), Schmitz (2005) qualitatively described the role and interactions of these various types of LCFEs (located west, east and north of the LC) on the LCE shedding sequence.

Model simulations have been widely used since the 1980's to study GoM dynamics, in particular LCE shedding. Model studies of the GoM dynamics have been described by Oey et al. (2005). Among those, few studies focus on the LC frontal dynamics. Using an isopycnic model, Chérubin et al. (2006) found that the anticyclonic LCE and the surrounding cyclonic LCFEs tend to form a multi-pole which is advected westward and is influenced by the local topography. Oey (2008) studied deep cyclones in the eastern GoM in a model simulation and identified locations for cyclogenesis through baroclinic instabilities, at all depths north of CB and along the West Florida Shelf near the surface and in the deepest layers. These simulated instabilities are phased with the LC extension and shedding. However, these local instabilities have never been specifically isolated in observations so far. Using a hybrid model, Le Hénaff et al. (2012b) found that LCFEs are intensified in the northern GoM through topographic interaction when they flow over the Mississippi Fan, which is the smoothest part of the northern GoM shelf slope (Figure 1). This intensification is due to the entrainment, by an incoming small LCFE, of water parcels from the shallower Mississippi Fan area toward the deep northeastern GoM, leading to vortex stretching and vorticity intensification. Although qualitatively noted on altimetry or SST maps, this intensification has never been properly characterized based on observations. Le Hénaff et al. (2012b) also noted that the sharp topography at the northeastern corner of the GoM favors the blocking of LCFEs between the West Florida Shelf and the LC, leading to eddy merging with incoming cyclones. This blocking is consistent with results by Walker et al. (2009, 2011). In particular, Walker et al. (2011), based on altimetry maps, identified a LCFE that remained nearly stationary for months in the northeastern GoM during the Deepwater Horizon oil spill period.

The use of altimetry maps is well adapted for studying the LC or LCEs, which are large (200 to 400 km diameter). However, despite their use in qualitative studies (Schmitz, 2005), these maps are not well adapted for the precise characterization of the LCFEs, whose size is smaller. Based on wavelet analysis, Dussurget et al. (2011) showed that, in the Bay of Biscay, global altimetry maps were not able to precisely characterize the size and amplitude of eddies smaller than 130 km (see their Figure 8); that limit is related to the decorrelation scales of about 125 km used to produce global maps at these latitudes (Le Traon et al., 1998). In particular, the altimetry-mapped data lead to an overestimation of the size, and an underestimation of the amplitude, of smaller eddies (Dussurget et al., 2011). In the GoM, altimetry-based SSH maps are derived with decorrelation scales of 100 km minimum (Leben, 2005), which means that LCFEs, whose scales are between 80 and 120 km, are probably not well represented in such products. Along-track altimetry data is thus better adapted for the robust characterization of LCFEs in the GoM interior.

Along-track altimetry data have already been used for analyzing LCFEs, but only for isolated events (Zavala-Hidalgo et al., 2003, Walker et al., 2009). Walker et al. (2009) used along-track altimetry data to complement SST maps and drifter trajectories. Analyzing the evolution of LCFEs between 2001 and 2004 (excluding summer periods), they detected episodes of coalescence of some LCFEs around the LC edge, and confirmed the general growth of LCFEs along the LC pathway.

Similarly to altimetry, ocean drifter data so far have been used mainly to describe the ocean dynamical field at the global or basin scales (e.g. Griffa et al., 2008, Lumpkin and Elipot, 2010). Drifter data are especially adapted for studying the ocean eddy field, in particular the rotation rate or spin (Veneziani et al., 2004). Inside the GoM, the shelf circulation was studied with drifters released over the Texas-Louisiana and Florida-Alabama shelves during the Surface

Current and Lagrangian Drift Program (SCULP, LaCasce and Ohlmann, 2003; Ohlmann and Niiler, 2005). However, there is no study, to our knowledge, that specifically examines the eddy field of the deep GoM based on drifter data despite the long history of such observations, which have been primarily obtained through the Global Drifter Program (GDP, Niiler et al., 1995). In the GoM interior, drifter data seem to have been used only to complement other data in describing individual events (e.g. Walker et al., 2009; 2011).

The first objective of this paper is to use the most reliable information from almost 20 years of along-track altimetry observations and long-term GDP drifter dataset to provide new insights on the LCFE activity in the GoM. The second objective is to study whether recent results from model studies dedicated to LCFEs, especially the eddy intensification in the northeastern GoM described in Le Hénaff et al. (2012), and the favored baroclinic instability identified in specific locations by Oey (2008), can be confirmed with observations from along-track altimetry and drifter trajectories. The third objective is to use our ~20 year long dataset to derive updated estimates of LCFE characteristics, which were previously estimated based mostly on a few years of limited SST maps, and to complement our knowledge about LCFE activity in the GoM. A last objective is to compare results from both datasets, in order to evaluate the robustness of the results.

In Section 2, we describe the along-track altimetry dataset and the methodology used to derive eddy characteristics, and we present an analysis of the mean LCFEs characteristics, in relation with the LC extension inside the GoM. In Section 3, we present the GDP data set, the methodology used to derive maps of the mean rotation field of the GoM, and we analyze the results in relation with the results from the along-track altimetry analysis. In Section 4, we use high resolution SST maps and altimetry to specifically analyze a period during which a surface

drifter is entrained in cyclonic loops for a long period. The drifter trajectory is examined in detail, to analyze the associated vorticity field and to compare estimates from this trajectory and from along-track altimetry. Finally, Section 5 presents the conclusions.

2. Analysis of altimetry data

2.1 The altimetric dataset

We first employ altimetry data to describe the cyclonic activity in the eastern GoM basin, east of 90°W. The along-track data used for this study are Sea Level Anomaly (SLA) from the AVISO dataset. We use the updated, delayed time data, which benefit from higher quality treatment of the raw altimetric signal. In addition, we use the "vxxc" data, which are not filtered, nor sub-sampled (MyOcean Sea Level SLA products, Larnicol et al., 2011), to ensure the data contain the least altered information possible. SLA data from all altimeters in orbit between October 1992 and January 2011 are considered. This includes Topex/Poseidon, GFO, Jason 1, Envisat and Jason 2, with the periods of interleave orbit at the end of Topex/Poseidon and Jason 1 missions. Topex/Poseidon and the Jason series have a repeat period of 10 days for each track, while GFO has a repeat period of 17 days and Envisat has a period of 35 days. Figure 2 shows the various altimeter tracks included in our study. The reference tracks from Topex/Poseidon and the Jason series provide data during the whole study period, while the interleaved tracks from Topex/Poseidon and Jason 1 provide data for the periods September 2002 – October 2005 and February 2009 – January 2011, respectively. GFO data cover the period January 2000 – August 2008, and Envisat data cover the period October 2002 – November 2010. The period from

September 2002 to October 2005 is the richest one in data, with four altimeters in orbit (Topex/Poseidon, Jason 1, GFO and Envisat) for more than 3 years.

Since SLA is estimated in comparison with the average of sea level measurements by the satellite, it does not contain the constant part of the ocean total Sea Surface Height (SSH), called the Mean Dynamic Topography (MDT). This is problematic in our study area, because the LC is an intense current with a large SSH signature. In the eastern GoM, where the LC extends and retracts, a positive SLA is usually associated with the presence of the LC (or a newly detached anticyclonic ring), while a negative SLA can be associated with the absence of the LC. Since cyclones are also associated with a depression in sea level, there could be confusion between negative SLA due to a cyclone, or to a period of LC absence. We overcome this problem by using the Centre National d'Etudes Spatiales CNES-CLS09 MDT map from Rio et al. (2011), from which we extract the MDT values along the satellite tracks. These values are added to the along-track SLA to form the along-track total SSH. Hence, the LC and associated anticyclonic rings are associated with large values in SSH, while LCFEs are associated with SSH lows.

We only consider data in the part of the GoM that is deeper than 150 m. This value is a trade-off between the necessity of ignoring data on the continental shelf, where the SSH signal has large variability not expected to be associated with cyclones, and the frequent proximity of LCFEs to the shelf break, especially along the West Florida Shelf.

We perform a wavelet analysis to isolate and characterize LCFEs on along-track SSH. This wavelet analysis and the methodology to estimate eddy center, diameter, amplitude, and surface relative vorticity for each eddy are presented in Appendix A, along with the criteria for gathering the LCFE dataset derived from altimetric measurements. The wavelet analysis is

adapted from Dussurget et al. (2011) for our study zone and is extended to derive the eddy relative vorticity at the surface.

2.2 Results

2.2.1 Average maps

Figure 3 shows maps synthesizing the results from the along-track analysis. All quantities estimated for each cyclone identified along individual tracks have been attributed to a single point at the location of the eddy center, and these quantities have then been averaged in bins of 1/3° resolution. This bin size allows a fine enough spatial resolution to clearly identify regions of interest, while keeping a sufficiently large number of observations in each bin to calculate meaningful averages. The first map (Figure 3a) shows the density of observations, which is estimated in each bin as the ratio between the number of observed eddies and the number of individual satellite passes over that particular bin. The following maps (Figures 3b,c,d) show the average values of diameter, amplitude and relative vorticity, estimated from the wavelet analysis (see Appendix A). Figure 3e shows the distance between the detected cyclone and the LC or a LCE, which is estimated for each cyclone individually. Along each track, the presence of the LC or a LCE is identified when SSH is larger than a threshold value of 17 cm (Leben, 2005); the minimum distance between the eddy center and the location where the along-track SSH crosses that 17 cm threshold value defines the distance to the LC or a LCE. On each panel, a typical pathway of the extended LC (adapted from Vukovich, 1988) has been added to help interpret the data.

The occurrence of observed cyclones (Figure 3a) shows a larger cyclone density at the edge of the LC, when it is in extended position. The high density of cyclones is clearly following the LC pathway from the north of the CB to the GoM exit at the Straits of Florida, with two noticeable patches of higher cyclone observation frequency. The most intense of these patches is located in the area where Tortugas Eddies are usually observed (Fratantoni et al., 1998; see also Figure 1). These cyclones were noted to be quasi-stationary close to this location, based on 3-year radiometer measurements (Fratantoni et al., 1998). Here, we confirm that this specific location is associated with repeated observations of cyclones, based this time on almost 20 years of altimetry data, indicating a tendency for cyclones to stay there for extended periods of time. The second area of high cyclone occurrence is located in the deep northeastern GoM, around (86°W; 27°N). The high observation density here indicates that eddies tend to stay in this specific area for longer periods compared to other locations along the LC edge. This is consistent with results by Walker et al. (2011) at the time of the Deepwater Horizon oil spill, during which a LCFE remained in the deep northeastern GoM for about four months, trapped between the steep West Florida Shelf and the extended LC; in that situation, the LCFE aggregated other incoming cyclones from the LC edge, which leads to eddy merging and eddy growth. Such a process was also mentioned by Le Hénaff et al. (2012b), after the analysis of a LCE shedding sequence from a model simulation. Their results, which were based on individual episodes, are thus supported by statistics derived from our ~20 year long altimetry dataset.

The map of the estimated cyclones' diameter (Figure 3b) shows large values in the central and eastern parts of the study zone, corresponding to the deep central and deep eastern GoM. Along a typical LC pathway, the mean diameters are 80 to 100 km on the western side of the LC, from 25°N to 27°N, while they are 100 to 120 km on the northern and eastern side of the LC.

This is consistent with values found by Vukovich and Maul (1985), and confirms the tendency, noted by Vukovich (1988), of frontal eddies to have larger dimensions east of the LC compared to west of the LC. In addition to these estimations along the LC front, the dataset shows values of 120 km or more in a large area centered on (86.5°W; 25.5°N), and in a smaller area to the south, around (85°W; 24°N). These areas are in a part of the study zone where the density of observations is the lowest, as seen in Figure 3a, indicating that they are less commonly found than values along the LC pathway.

The map of cyclones' amplitude (Figure 3c) shows features similar to the diameter distribution (Figure 3b). The two areas around (86.5°W; 25.5°N) and (85°W; 24°N) associated with large diameter values also present large amplitude values. Similarly, the cyclones' amplitude grows along the typical pathway of the LC, the cyclones being associated with more pronounced SSH lows on the northern and eastern sides of the LC compared to the western side. A noticeable feature in Figure 3c is the large eddy amplitude in the deep northeastern GoM, around (86.5°W; 27.5°N). This corresponds to the area where the LC reaches the deep part of the GoM, after having flown over the Mississippi Fan; the boundary of this patch of larger amplitude clearly follows the 3000 m isobath. This signature is consistent with eddy intensification related to the specific northern GoM topography, in agreement with the mechanism proposed by Le Hénaff et al. (2012b): the incoming LCFEs advected over the Mississippi Fan entrain local water parcels toward the deeper area located in the northeastern GoM, which leads to vortex stretching and eddy intensification.

The larger cyclone amplitudes in the deep northeastern GoM also coincide with a local maximum in relative vorticity, as seen in Figure 3d. Cyclones detected in the northern GoM between 85°W and 88°W (at 27°N) are usually in proximity to the LC or a LCE, as shown in

Figure 3e, compared to the surrounding areas on the West Florida Shelf slope or toward the northern and western GoM. This indicates that cyclones detected there are mostly LCFEs. The local maximum in relative vorticity in the deep northeastern GoM is another indication, complementary to the cyclones' amplitude, that these LCFEs tend to intensify when they are advected along the northern edge of the extended LC. In Le Hénaff et al. (2012b), the intensification in surface relative vorticity due to the topographic effect of the Mississippi Fan was estimated to be about $0.1\,f \approx 0.6\text{-}0.7*10^{-5}$ s^{-1}. This is the order of magnitude of the difference in cyclones' average relative vorticity observed here between the deep northeastern GoM and the Mississippi Fan areas along the LC pathway. Altimetric observations of cyclones' amplitude and relative vorticity thus tend to confirm results from the modeling study of Le Hénaff et al. (2012b).

Further south along the LC pathway, on the east of the LC, the cyclones' relative vorticity is observed to have values close to $3*10^{-5}$ s^{-1}, from 27°N to 25°N (Figure 3d). South of that latitude, a large patch of intense relative vorticity extends into the deep GoM, reaching areas of observed large diameter and amplitude for cyclones, around (85°W; 24°N) as noted previously (Figures 3b and 3c). Large values of relative vorticity are also noticed along the shelf slope northwest of Cuba, around (84.5°W; 23°N), but this feature is associated with low observation frequency (Figure 3a), small eddy diameter (Figure 3b) and amplitude (Figure 3c). Thus, this specific feature may not be robust. Finally, the whole area on the slope of the CB north of 23°N generally shows large values of cyclones' relative vorticity, while the observed diameters were rather small, as expected from Vukovich (1988) on the west of the LC, and the amplitude of the cyclones is usually of intermediate values.

The above results, which are based on time-averaged values, will now be analyzed and interpreted in relation with the LC stage inside the GoM.

2.2.2 Influence of the LC extension

Figure 4 shows a map of the eastern GoM with various sub-domains delimited, each of which corresponds to an area of interest mentioned in the previous section. These areas were also shown in Figure 3. Figure 5 shows the distribution of the LC northern extension at the time of cyclone detections, as well as the associated relative vorticity, in each of the domains defined in Figure 4. The LC northern extension is estimated from AVISO Maps of Absolute Dynamic Topography (MADT) during the study period. Mapped products are necessary to identify the LC contour and derive its northern extension; our along-track dataset could not be used for this purpose. Specific trends in the distribution are identified by comparison with the distribution of the LC extension at all times, which is shown for all domains in Figure 5. The mean value of the LC northern extension is 26.0°N, close to the value given by Leben (2005), who found 26.2°N using a slightly different, shorter dataset.

The areas covering the Mississippi Fan and the deep northeastern GoM show comparable distributions of LC northern extension, although they showed different characteristics in eddy amplitude and relative vorticity in the previous section. In both locations, most of the observations occur when the LC extends beyond 26°N, which is consistent with the finding that cyclones detected in these two areas are frontal eddies, as shown previously by the average distance to the LC or LCE (Figure 3e). The large values for the LC northern extension in Figures 5a and 5b indicate that the cyclones in these two areas are essentially frontal to the LC *before* it

detaches or separates. In addition, the relative vorticity of these cyclones is larger when the LC extends beyond 26°N, meaning that the cyclones responsible for the dominant signal in average relative vorticity (Figure 3d) in these two areas are also frontal to the extended LC. The specific comparison between the two areas confirms a tendency for more intense relative vorticity in the deep northeastern GoM compared to the Mississippi Fan area, as seen in the average value maps presented in the previous section.

Further south along the LC pathway, the area noted as deep eastern GoM shows a different distribution (Figure 5c). Although the dataset includes many periods when the LC extends beyond 26.5°N, the majority of cyclones are observed when the LC does not extend north of 26.0°N. Considering the short distance between the LC or LCE and cyclones in that area (Figure 3e), these cyclones are essentially frontal to either the LC or a LCE. Cyclones associated with a LC extension south of 26.0°N can thus be frontal to either a newly detached or separated LCE, or to the retracted LC. Largest values in relative vorticity in that area are noticed when the LC extends either north of 26.0°N, i.e. before a detachment or separation, or around 24,5°N to 25°N, which is typical after a LCE detachment/separation.

The bimodality noted in large relative vorticity values in the deep eastern GoM area is more obvious in the area just south of it which we call deep southeastern GoM (Figure 5d). There, cyclones are usually observed either when the LC is well extended, i.e. north of 26.5°N, or when it has just retracted, with typical values south of 24.5°N. This marked bimodality is due to the fact that many LCE detachments or separations take place under the influence of LCFEs that are located in *this* particular area. These LCFEs first shrink the zonal extension of the LC from one or two sides, i.e. leading to a neck shape of the LC, before chopping the LC tip. This "necking down" effect usually involves one frontal eddy coming from the east of the LC, but an

eddy formed or intensified along the CB may also take part in the process (Zavala-Hidalgo et al., 2003, Schmitz, 2005, Le Hénaff et al., 2012b, Athié et al., 2012). At the time of a LCE detachment or separation, the LC extension suddenly drops from a large value to a very low one, explaining the occurrence of the two observed peaks. Figure 5d also indicates that many cyclones observed in the deep southeastern GoM have intense relative vorticity, which makes them more likely to play a role in LCE detachment or separation. In addition, the relative vorticity values observed in this area are usually larger than the values observed in the northern and eastern GoM, upstream of the LC pathway, for both extended and retracted modes.

Compared to other areas of the GoM upstream of the LC, the larger relative vorticity observed in the deep southeastern GoM is hard to interpret based on altimetry data only. This is partly due to the poor coverage of this area by the reference Topex/Poseidon-Jason tracks (Figure 2), associated with low observation frequency there (Figure 3a). However, considering that at least some of the cyclones observed in the deep southeastern GoM originate from the northern GoM and follow the LC pathway (e.g. Fratantoni et al. 1998), and that not all the cyclones from the northern GoM reach the southern GoM (some of them staying north before being advected westward to the GoM interior, together with a LCE, e.g. Walker et al. 2009), two scenarios might explain the large relative vorticity observed in the deep southeastern GoM: first, cyclones advected from the northern GoM are intensified locally in the deep southeastern GoM; second, only northern GoM cyclones with intense relative vorticity reach the deep southeastern GoM. Although it is not possible to estimate which scenario is most likely based on altimetry data alone, the drifter dataset will allow us to analyze in more detail a case of a frontal cyclone reaching the deep southeastern GoM (Section 4).

The deep central GoM area is the part of the GoM where the largest mean cyclone diameters are observed (Figure 3b), as well as large amplitude (Figure 3c), but it has no clear signal in relative vorticity (Figure 3d). This is an area with low frequency of cyclone observations (Figure 3a), although these cyclones tend to be frontal to the LC or a LCE (Figure 3e). The distribution of LC extension (Figure 5e) shows that the cyclones are observed almost exclusively when the LC is retracted to the south. This indicates that the cyclones observed in the deep central GoM are either frontal to a young LC, or to a LCE that has just detached. This area coincides with the location of cyclones that are able to block the LC extension when the LC is in the port-to-port situation (Zavala-Hidalgo et al., 2002, 2006). These cyclones are usually large: based on altimetry SSH maps, Zavala-Hidalgo et al. (2002) found such a cyclone centered on (86.5°W; 25.5°N), with a 200 km estimated diameter. This is consistent with our dataset: 8 of the 10 largest cyclones observed in the deep central GoM area with diameters larger than 150 km are detected when the LC extends south of 25.1°N, which is a southern (retracted) LC extension. These cyclones are associated with large amplitudes of 15 cm or more, but with rather low relative vorticities, less than $2.5*10^{-5}$ s^{-1}. In our dataset, some of these large diameters are detected in the early stage of the extension of LCE "Sargassum" that separated in 2003 after 509 days, which is an unusually long separation period for a LCE (Lugo-Fernandez and Leben, 2010). This is consistent with the findings from Zavala-Hidalgo et al. (2002, 2006), who found that such large cyclones were associated with blocking of the LC. Large values are also observed during detachment of LCE "Vortex" in spring 2005 (Lugo-Fernandez and Leben, 2010) before the LC was able to re-attach with the detached LCE (not shown). Finally, other episodes of large cyclones are observed directly after LCE separation: after LCE "Ulysses" in 2004, and LCEs "Darwin" and "Ekman" in 2009 (Lugo-Fernandez and Leben, 2010). In these last three cases, the large cyclones did not lead to actual blockage of the LC, although they showed characteristics of

blocking cyclones, i.e. large diameter and amplitude. Large cyclones in the deep central GoM are thus not always associated with blocking of the LC extension, which was previously commonly believed. These cyclones are the dominant signal in the deep central GoM in our altimetric dataset.

The Dry Tortugas area has the highest density of observations (Figure 3a). The associated LC extension distribution (Figure 5f) indicates that these cyclones are almost exclusively observed when the LC extends north of 25.5°N, meaning that Tortugas Eddies are observed only when the LC is extended into the GoM. Tortugas Eddies are associated with a weaker relative vorticity than observed in the deep southeastern GoM area, from where they are thought to have migrated (Fratantoni et al., 1998). Figures 3b, 3c and 3d show no consistent signal in either diameter, amplitude or relative vorticity in the Dry Tortugas area. In particular, all these quantities are lower in the Dry Tortugas area than in the deep southeastern GoM. This indicates that the LCFEs that form Tortugas Eddies are modified either during their migration from the deep southeastern GoM to the Dry Tortugas area, or inside that area. This result extends findings from Fratantoni et al. (1998) and Kourafalou and Kang (2012), who found that Tortugas Eddies experience changes in their shape and kinematics when they are advected inside the Straits of Florida. Our analysis suggests that the LCFEs that form the Tortugas Eddies have already experienced changes before entering the Straits of Florida.

Over the slope of the CB, the northern area shows quite large observation frequency in the northern tip of the CB slope and in the deep region immediately north of the slope (Figure 3a). This area is associated with large values in relative vorticity (Figure 3d) and is consistent with an area of intense baroclinic instabilities along the LC pathway identified in a numerical simulation by Oey (2008), both near the surface and in deeper layers. Our altimetric dataset thus confirms,

for the first time, the presence of cyclones with large vorticity, as expected from the modeling study by Oey (2008). The general distribution of LC extensions at the time of cyclone observations in the area is quite close to the reference distribution of the LC extension over the data period (Figure 5g), and also with generally large values for relative vorticity. However, the largest values in relative vorticity show bimodality, with observations either when the LC extends north of 26.5°N, or south of 26.0°N. This bimodality is comparable to the one noticed in the deep southeastern GoM, and suggests that the locally most intense LCFEs are involved in LCE detachment or separation, here taking place along the northern edge of the CB. This is consistent with the phasing of local baroclinic instabilities with the LC extension-retraction cycle involved in the LCE shedding sequence (Oey, 2008). This might also explain why the relative vorticity detected over the CB slope is on average larger than on the Mississippi Fan further north, as the most intense cyclones did not reach the northern GoM after they took part in a detachment.

Finally, Figure 5h shows the distribution of LC extension associated with LCFEs for the eastern CB. This is an area of low observation frequency (Figure 3a) with small to intermediate cyclone diameters (Figure 3b) and locally large amplitude and relative vorticity (Figures 3c and 3d), especially in the region close to the deep southeastern GoM area. The distribution of LC extension shows preferred occurrences of cyclones when the LC is retracted, despite the fact that the LC is always flowing inside this area. This means that the presence of cyclones is not related to the presence or absence of the LC itself. The observed peak at very low latitudes indicates a favored tendency for eddy presence when the LC has just retracted, following LCE detachment or separation. Zavala-Hidalgo et al. (2003), Schmitz (2005) and Athié et al. (2012) noted that frontal eddies along the CB are commonly involved in a LCE shedding sequence. Their results are complemented by our analysis, which suggests that these LCFEs are detected preferably *after* a

LCE detachment. LCFEs can thus play a role in a future detachment or separation only after the re-attachment of the initial LCE. Such a sequence involving several detachments and re-attachments, initiated by a LCFE east of the LC and later supported by a LCFE formed or intensified along the CB, was noticed for a LCE shedding sequence in altimetry maps, as well as in a numerical simulation (Le Hénaff et al., 2012b).

Some of the aspects and hypotheses concerning LCFEs as observed by altimetry data will now be investigated using surface drifter data, which provides complementary information on the vorticity field in the eastern GoM.

3. Analysis of drifter data

3.1 The drifter dataset

We now look for the signature of frontal eddies in surface drifter data. We use the data from the Global Drifter Program (GDP). This program, following the Surface Velocity Program (SVP) started in 1979, aims at providing measurements of near-surface ocean currents worldwide at 15 m depth (Niiler et al., 1995, Reverdin et al., 2003). To do so, SVP drifters are composed of a spherical buoy at the surface, connected to a nylon holey sock drogue (sea anchor) so that the drifting system tracks the water displacement at 15 m (Lumpkin and Pazos, 2007). Drogue presence was determined as described in Lumpkin et al. (2013). The global drifter array is managed by NOAA's Atlantic Oceanographic and Meteorological Laboratory (AOML), with the objective of maintaining global 5°x5° world ocean coverage, corresponding to approximately 1250 drifters simultaneously at sea. Although GDP deployments have primarily been conducted in the open basins, the dataset provides useful data in the GoM. Figure 6 is a map showing all the

trajectories from the 148 GDP drifters transiting through or deployed in the GoM from 1993 (the earliest observation) to 2011. The GDP provides the drifter positions and dates interpolated to regular 6 hr intervals, along with the associated velocity vectors estimated as 12 hrs centered differences, and the measured SST. The highest density of observations is reached along the Caribbean Current south of the Yucatan Channel, in the Florida Current and the Gulf Stream east of the GoM, and in the eastern GoM. There, drifter data cover a wide area corresponding to the various stages of the LC extension inside the GoM. Although the observation density is lower, some of the GDP drifters also reach the western GoM. Drifters are usually not advected over the continental shelf. The contrast in observations density between the CB shelf (shallower than 200 m), which is quite clear from trajectories, and the deeper part of the GoM indicates how the LC, just north of the Yucatan Channel, follows the shelf break to reach the interior GoM.

Among all the GDP observations available inside the GoM, 52% are taken after the drifter lost its drogue. This loss affects the drifter trajectory and makes it directly sensitive to the surface wind (Grodsky et al., 2011). However, winds are usually light in the GoM, and many trajectories of undrogued drifters are clearly useable for studying the GoM dynamics. For this study, NCEP operational wind vectors were interpolated to the drifter positions. Appendix B describes how we derived an extended drifter data set based on the analysis of the wind field and drifter trajectories. The methodology used to extend the drifter dataset can be used in any area where the impact of the winds on the drifter trajectories is expected to be small, such as the subtropics and the tropics. Figure 7 shows the number of daily drifter observations in the GoM, for drifters with their drogue on only, and for drifters from this extended data set. The total number of individual 6 hr observations increased from 24,101 (drogue on only) to 43,143 (extended data set), i.e. a 79%

increase. This data set thus allows us to make better use of available data, and extend the statistical meaning of our results.

The extended dataset (Appendix B) is used to estimate the rotation experienced by the drifters depending on their location in the GoM. To do so, we calculate for each drifter trajectory the spin Ω (Borgas et al., 1997), which represents the mean rotation per time interval along the trajectory (Veneziani et al., 2004, Griffa et al., 2008): $\Omega=\langle u'dv' - v'du' \rangle/(2\Delta t\ EKE)$, where u' and v' are the anomalies of drifter velocities with respect to the mean flow, Δt is the time sampling interval for velocities, here 12 hrs, and EKE is the Eddy Kinetic Energy: $EKE=0.5\ \langle u'^2 + v'^2 \rangle$). The mean flow from which to calculate velocity anomalies u', v' and EKE is taken as the average, from 1993 to 2011, of the geostrophic velocities estimated from altimetry. We used the 1/3° mapped AVISO products to calculate that mean current value. Tests were also performed using a mean flow estimated directly with the currents from the GDP drifter dataset, and showed similar results to those presented here. Non-zero values for the spin are associated with cyclonic ($\Omega>0$ in Northern hemisphere) or anticyclonic ($\Omega<0$) motions of the drifter. Large values of the spin are associated with drifter looping and spiraling; trajectories presenting such features are often referred to as loopers (Richardson, 1993, Griffa et al., 2008). When the drifter is in the core of a coherent eddy, the spin value provides a good estimate of the relative vorticity ζ ($\zeta \sim 2\Omega$, Veneziani et al., 2005).

In the present study, we are especially interested in positive spin values associated with cyclonic frontal eddies. In the GoM, the spin value at every point along each trajectory is estimated over a time interval that has to be consistent with the typical period of mesoscale activity with a rotation signature, such as mesoscale eddies. This period is estimated from the

trajectory shown on Figure B1e, which is by far the longest sample of a drifter trapped in a mesoscale eddy in the GoM dataset, and the longest inside a LCFE to our knowledge; rotation periods are between 3 and 4 days, so we set the averaging period at 3.5 days.

3.2 Results of drifter analysis

As we wish to use the GDP dataset to estimate the average spin state, we have to consider the density of drifter observations in our dataset. Figure 7 shows that there are usually less than 10 daily drifter observations in the GoM, with some exceptions. The first period of dense observations took place during the international Year of the Sea, from late 1999 to early 2001, with daily observations reaching 30 to 40. The second dense period of observations happened in late 2008 for a few weeks, again reaching 30 to 40 observations per day. The last period of high measurement density follows the Deepwater Horizon oil spill in April 2010. For about 6 months, daily drifter observations exceed 40, and they exceed 60 during the 3 summer months. This period is by far the time of highest observation density in the GoM, which leads to a potential bias: among the 43,143 GDP individual observations available in the GoM, 14,992 (i.e. 35%) were taken in the months following the Deepwater Horizon oil spill. In terms of ocean processes, this period is characterized by the very prolonged shedding process of LC Eddy "Franklin", with many detachments and re-attachments (Hamilton et al., 2011). In particular, Eddy Franklin stayed in the area centered on (88.5°W; 25°N) for weeks, as seen in Figures B1a,c, while the LC stayed mostly retracted, re-attaching and detaching from the LCE several times. In order to avoid biasing the results toward this specific GoM situation, we decided to discard observations from the period following the Deepwater Horizon oil spill before deriving the map of mean spin over the GoM.

Figure 8a shows the map of mean spin calculated over the eastern GoM, without considering data after April 2010. The map was derived by applying the clustering technique described by Koszalka and LaCasce (2010), which is especially adapted for plotting results from drifter data. The main idea of the clustering technique is to gather data in groups of the same number of observations, whatever the spatial density of observations in each cluster might be. The clusters' composition and centers are estimated in an iterative process, in which the location of the center of each cluster is updated to reach an optimal criterion of cluster composition and minimum distance of each observation to its cluster center (see Koszalka and LaCasce, 2010, for more details). In the present study, we estimated such clusters for the GDP data in the GoM, each one grouping 50 observations. This value is close to the value of 45 chosen by Koszalka and LaCasce (2010) to reach a fine resolution for plotting their results. The mean value of the spin Ω from all observations in each cluster is then collocated at the cluster center. We discarded clusters that contained data from less than 3 different drifters, in order to prevent a strong bias from individual trajectories; this only affected clusters at the periphery of the GoM. Finally, the outputs have been plotted on a regular grid of 0.1° resolution.

The map in Figure 8a shows several patches associated with cyclonic or anticylonic motion. The most intense patch of cyclonic spin is located on the shelf break south of the Mississippi Delta, away from the LC extension area we are interested in. Focusing on the LC extension zone, generally south of 28°N and east of 89°W, the most intense cyclonic spin features coincide with areas of interest previously noted in the analysis of along-track altimetry data. The first feature is located in the deep northeastern GoM, where cyclones were found to be larger in size and amplitude, and more intense in relative vorticity, compared to cyclones observed over the Mississippi Fan upstream of the LC pathway; cyclones were also observed

more frequently there in altimetry (see Section 2.2). Results from drifter trajectories indicate intense cyclonic motion in that area, which is consistent with either intensification of the cyclones' rotation when they reach that area, or with longer presence of cyclones (compared to other areas), or both. Indeed, several trajectories show loopers in that particular area, whereas no looper is observed over the Mississippi Fan. Among these trajectories, some clearly follow the LC pathway, initially straight (non-looping) as they move toward the northern GoM, then over the Mississippi Fan, and then they start to loop after arriving at the deep northeastern GoM. The trajectory from drifter #40430 is typical of such behavior (Figure B1e). This behavior might be due to the fact that, prior to the drifter reaching the deep northeastern GoM area, the cyclonic vorticity along the LC was not strong enough to entrain the drifter in a looping movement. This is consistent with a local intensification of LCFEs over the Mississippi Fan, due to vortex stretching of water parcels entrained toward the deep northeastern GoM by the incoming LCFEs, as analyzed in a modeling study (Le Hénaff et al., 2012b). Based on the results presented herein, it is the first time that this intense and very localized cyclonic activity is quantified in the northern GoM with *in situ* observations. Our results also demonstrated intense cyclonic relative vorticity in the deep northeastern GoM based on altimetry data (see Section 2.2). The second patch of intense cyclonic spin is located in the deep southeastern GoM (Figure 8a), where altimetry-observed cyclones were found to have large diameter and very intense amplitude and relative vorticity, although they were not observed frequently (see Section 2.2). Thus, these two patches of cyclonic spin are consistent with the results based on along-track altimetry.

In order to evaluate the impact of discarding data past April 2010, Figure 8b also shows the average spin calculated over the entire dataset. This map shows comparable features, but with altered amplitude: the positive spin patch in the deep northeastern GoM is less intense, although

still present, whereas the positive patch in the deep southeastern GoM extends northwestward, still with large intensity. This dominant positive patch is the result of the specific characteristics of the GoM mesoscale circulation during the summer of 2010, which was intensively observed by GDP drifters compared to previous years (Figure 7). During this period, LC Eddy Franklin detached and re-attached several times, associated with the presence of LCFEs between the base of the LC and detached Eddy Franklin, as observed in the early stage of drifter #98911 (Figure B1a). The signature of Eddy Franklin is also visible in Figure 8b with the patch of positive spin centered on (88.5°W, 25°N), which is the location of anticyclonic loops on drifter trajectories (such as drifters #98911 and #98949, Figures B1a,c), but was not present in the spin average estimated with data prior to April 2010 (Figure 8a).

As previously mentioned, the patch of positive spin in the deep southeastern GoM noted in Figures 8a and 8b coincides with the area of intense relative vorticity observed in along-track altimetry, but for which the observation frequency is very low. In the drifter dataset, there is at least one occurrence of cyclonic loopers in that area from drifter #40430 (Figure B1e). That trajectory exhibited cyclonic looping for months and provides the longest single trajectory in a LCFE inside the GoM in our dataset. In addition, it is clear from its trajectory that the drifter sampled several cyclonic loops in both the deep northeastern GoM and the deep southeastern GoM, where patches of intense positive spin have been identified (Figure 8a). Therefore, we also plotted the average spin calculated with data prior to April 2010, while also discarding data from that particular drifter (Figure 8c). Compared to Figure 8a, the patch of intense positive spin in the deep southeastern GoM almost disappears, but the one in the deep northeastern GoM is only slightly modified and remains quite intense. This indicates that the patch of positive spin in the deep southeastern GoM is due to infrequent but intense events. From the analysis of altimetry

data, these events are associated with LCE detachment or separation. In contrast, the patch of positive spin in the deep northeastern GoM is a more robust feature, based on repeated observations in both the drifter and altimetry datasets.

One of the most noticeable discrepancies between the drifter and altimetry results is the absence of a signal clearly related to the Tortugas Eddies in the drifter data. Despite their intense sampling in altimetry, only a few drifters were trapped in a cyclone in the Dry Tortugas area, although numerous drifter trajectories were deflected to the south in that area, which is an indirect indication of the presence of a Tortugas Eddy. The absence of strong cyclonic spin patch from the drifter dataset in that area may be due to the fact that most of the drifters that exit the GoM are advected by the LC in the Dry Tortugas area, including at times when the LC is not extended. Based on altimetry data, there is no Tortugas Eddy when the LC extends south of 25.5°N (Section 2.3). As a result, the spin estimate in the Dry Tortugas area incorporates drifter trajectories from periods of presence and periods of absence of a Tortugas Eddy. The presence of many laminar trajectories in that area tends to keep the mean spin there relatively low. Such dilution of the LCFEs' signature is not so prominent in the northern GoM; there, most of the drifters are advected by the extended LC, i.e. at periods when intense LCFEs are present locally (see Section 2.3), thus favoring the presence of marked cyclonic spin.

In addition to the Dry Tortugas area, discrepancies between the drifter and altimetry results are also present in the CB area, most of which is not associated with intense positive spin, as opposed to the intense relative vorticity generally found in altimetry data. Indeed, most of the drifter trajectories over the CB slope are laminar (following the LC pathway), with very few loopers, despite the density of trajectories there (Figure 6). In altimetry, the frequency of cyclone observations was very low over most of the CB slope (Figure 3a), but the observed relative

vorticity was quite intense. This observed large relative vorticity noted in altimetry is possibly due to the cyclone detection method: cyclones along the CB slope are usually of small dimension, being on the west side of the LC (Figure 3b, see also Vukovich, 1988). It is thus possible that the weakest of these small frontal cyclones are not detected, with amplitude below the amplitude threshold value used to identify cyclones based on the along-track spectrum (see Appendix A). This leads to keeping only eddies with small diameters but large amplitude and thus intense relative vorticity. Another possibility for the observed differences between the two datasets over the CB slope is that the drifters, while transiting in the Yucatan Channel and just north of it, are subject to an intense transport barrier formed by the LC itself, across which they cannot cross. This barrier might weaken slightly downstream, allowing drifters to cross it and sample the external edge of the LC. In addition, no drifter has been deployed west of the LC on the CB slope. This might explain why no cyclone is sampled in the CB area, leading to a very weak spin estimate. The existence of limitations in each data type supports an approach based on the combined use of altimetry and drifter data for accessing the most complete view of the local eddy field, as is done here.

Finally, in the drifter dataset, there is a small patch of positive spin just north of the CB slope, which is also an area of intense relative vorticity detected in altimetry, and which coincides with the area of baroclinic intensification noted by Oey (2008) in a model simulation. Its signature is not so intense in the drifter dataset, compared to other areas in the eastern GoM. This suggests that this location shows favored cyclonic activity which was more clearly seen in altimetry observations (Section 2.3).

4. Targeted study of a single drifter trajectory

4.1 Visual comparison with satellite SST and along-track altimetry

As noted previously, the trajectory of drifter #40430 (Figure B1e) is especially interesting in the context of studying LCFEs. The drifter started looping when it reached the deep northeastern GoM, after leaving the Mississippi Fan. This is consistent with results from along-track altimetry data analysis (Section 2.2), indicating an intensification of the LCFEs when they reach the deep eastern GoM coming from the Mississippi Fan, in agreement with the topography-induced vortex-stretching mechanism analyzed by Le Hénaff et al. (2012b). This is also consistent with results from the overall GDP dataset (Section 3.2), to which this drifter contributed, showing favorable cyclonic motion in the deep northeastern GoM. In the case of drifter #40430, the LCFE did not stay blocked in the deep northeastern GoM, but instead followed the edge of the LC from the northeastern GoM in early April 2004, to the southeastern GoM almost to the entrance of the Straits of Florida in late July 2004. As such, it provided data related to LCFEs continuously for almost four months. This is the first time, to our knowledge, that a drifter was embedded in a LCFE for such a long period of time. We thus wish to study this particular drifter trajectory in more detail. In addition, the period covered by this trajectory in 2004 is included in the period from September 2002 to October 2005 during which there were four altimeters in orbit (see Section 2.1). It is thus a favorable period for directly comparing the drifter trajectory with results from the along-track altimetry analysis.

We first compare the drifter trajectory to the SST maps from the Multiscale Ultrahigh Resolution (MUR) dataset from NASA, a product from the Group for High Resolution Sea Surface Temperature (GHRSST). This dataset has a global 0.011° resolution, and uses SST observations from several instruments, including the NASA Advanced Microwave Scanning

Radiometer-EOS (AMSRE) and the Moderate Resolution Imaging Spectroradiometer (MODIS) on the NASA Aqua and Terra platforms. It provides daily data starting on December 26, 2003. This very high resolution SST dataset is ideal for studying the front associated with the presence of LCFEs at the edge of the LC inside the GoM. Figure 9 shows several maps of daily SST from the MUR dataset, with the drifter trajectory up to that date superimposed. In addition, altimeter tracks associated with cyclones observed by altimetry, and corresponding to the loop described by the drifter on each date, have been added, with the location of the cyclone center and boundaries estimated from altimetry (see Appendix A).

In the initial stage of the looping phase in early April (Figure 9a), the LCFE was not clearly identified in SST, although the drifter had started looping and altimetry identifies a cyclone with center and boundaries in good agreement with the drifter trajectory. Two weeks later, on April 21, the LCFE was clearly associated with a cold signature in SST (Figure 9b). The drifter followed the SST gradient, while the altimetry estimate locates the cyclone boundaries slightly outside the strongest SST gradient. Twelve days later, on May 3rd, the drifter was located along the West Florida Shelf, further to the south (Figure 9c). As before, the drifter followed the strongest SST gradient, while the altimetry estimate located the cyclone boundaries slightly outside the intense SST gradient, although they were very close. Until that date, the three datasets show reasonable agreement.

Two weeks later, on May 18, the LCFE started elongating toward the southwest and the CB (Figure 9d), although there was no detachment of a LCE then (Leben, 2005). The SST gradient associated with the LCFE was still quite intense, but the drifter started migrating toward the cyclone center, and the loops formed by the drifter were smaller than the boundary visually estimated from SST. Along-track altimetry estimated an eddy center in agreement with the drifter

trajectory, which was close to the LCFE center; the boundaries estimated from altimetry were still slightly outside of the strongest SST gradient. Ten days later, on May 28 (Figure 9e), the analysis of the SST map had become difficult because SST had started increasing all over the GoM and would soon reach comparable values for both the LC and LCFEs, making them hard to distinguish. However, at that date it was still possible to identify the low SST associated with the LCFE. This SST signature shows that the size of the LCFE had decreased, and that it no longer reached the CB slope. As before, the drifter trajectory was very close to the eddy center. The center of the cyclone estimated by altimetry was still in agreement with the drifter trajectory, but the estimated boundaries tended to be further outside the SST gradient line, in the area of large temperature associated with the LC flow. In June, it became very challenging to identify the LCFE based on SST, and the altimetry analysis provided few observations to compare with the drifter trajectory. On Figure 9f, we notice that the drifter did many loops in June, close to the location it was in late May, before migrating eastward and starting looping cyclonically with a larger diameter. Unfortunately, we cannot identify an associated signal in SST. In addition, the along-track altimetry analysis indicates an eddy center that is far south of what seems to be the center of the loop followed by the drifter; the cyclone northern boundary is consistent with the drifter pathway, but the southern one is far to the south of the actual trajectory. The drifter continued looping for a few weeks, as it was entrained further south later in June and July (Figure B1e), but we decided not to include this part since we could no longer use SST maps.

This comparison between the drifter trajectory, SST and along-track altimetry analysis indicates that the drifter first tended to follow the strongest SST gradients associated with the LCFE boundary before migrating toward the eddy interior close to its center, and finally being entrained in larger cyclonic loops. The along-track altimetry analysis shows good agreement with

the drifter trajectory for the location of the eddy center and boundaries, especially in the early stage of the trajectory. The boundaries estimated from altimetry appear to be quite close to the strongest SST gradient, with a slight overestimation that is more marked when the LCFE was in the deep southeastern GoM.

4.2 Decomposition of the drifter trajectory into time-varying ellipses

The shrinking of the LCFE noticed in SST, and the abrupt changes in the drifter trajectory noticed between late May and late June, still remain to be explained. In order to have a better insight on that particular trajectory, we now use the drifter trajectory analysis tool developed by Lilly et al. (2011). This tool is based on the decomposition of a trajectory into the sum of time-varying ellipses and a residual, which represents the turbulent background flow as well as the non-oscillatory part of the flow. The time-varying ellipses are isolated based on a complex-valued wavelet transform of the trajectory. More details are explained by Lilly et al. (2011), who also provide free access to the numerical codes used for this analysis.

Figure 10 shows the decomposition of drifter #40430 trajectory into time-varying ellipses and residual flow. The ellipses are first elongated in the direction of the eddy and LC pathway, before migrating southwestward and decreasing in size, as seen in Figure 9. After many small loops in the central area, the drifter trajectory shows additional loops to the east and southeast which could not be studied in SST maps. The residual flow along the drifter trajectory shows oscillatory-like behavior, which is especially clear in the early stages of the looping. These features have a period close to the period of the cyclone rotation itself; in particular, they are not inertial oscillations. These undulations might be due to the fact that the LCFE is not exactly

elliptical in its motion. In particular, the part of the trajectory that is tangential to the LC, in the GoM interior side, shows much larger velocities associated with the LC, compared to other parts of each loop. The undulations thus represent a higher order term that is not captured by the ellipse decomposition model (Lilly, pers. comm.).

We now focus on the time-varying ellipses part of the trajectory estimated from the decomposition. The decomposition provides an evaluation of the ellipse radius and velocity along the elliptical part of the motion, for each drifter location. Figure 11a shows the drifter trajectory with the actual days during which the decomposition identified an ellipse-like displacement in the eddy trajectory. This period lasts from day 46 to 159 of the trajectory (April 1st to July 23rd, 2004). Figure 11b shows the instantaneous radius and velocity along the time-varying ellipses estimated from the decomposition. This figure clearly shows that the drifter sampled the characteristics of two cyclones, each with a distinct signature. These signatures are typical of a Rankine structure, in which the azimuthal velocity is proportional to the radius r for $r<r_0$, and decreasing as $1/r$ for $r>r_0$, r_0 being the core radius. This structure describes an eddy in solid body rotation, i.e. with uniform relative vorticity, inside the core radius. It is the first time, to our knowledge, that the solid-body rotation of a LCFEs has been observed. Solid-body rotation has been observed for other ocean eddies, although it is not the only profile possible. This characteristic has been observed for Meddies (Paillet et al. 2002), for mesoscale eddies in the North Equatorial Pacific Ocean (Flament et al., 2001) and in the Labrador Sea (Lilly and Rhines, 2002), or for North Brazil Current anticyclonic rings (Castelão and Johns, 2011).

Initially, the ellipse had a radius larger than 50 km, with a velocity of about 50 cm.s^{-1}. As the drifter followed the LCFE along the West Florida Shelf, the ellipse it described had a smaller radius, while the associated velocity slightly increased. There was an exception between days 75

and 85, when the LCFE started migrating southwestward toward the CB, during which time the velocity dropped as the radius decreased. After day 85 the characteristics of the eddy resumed the tendency of reduced radius and increased velocity, up to 80 $cm.s^{-1}$. Around day 90, as the radius has come down to about 35 km, the velocity started decreasing almost linearly with radius decrease, as sampled by the drifter. This is associated with solid-body rotation, with a slope equal to $\Omega = \zeta/2$, where ζ is the relative vorticity. For the first cyclone the relative vorticity is estimated to be $\zeta = 4.2 * 10^{-5}\ s^{-1}$, which is consistent with the values of quite intense eddies found in along-track altimetry (see Section 2.2). The Rankine-type profile estimated for the first cyclone is shown in Figure 11b.

The drifter kept following the solid-body profile associated with the first cyclone down to a radius smaller than 20 km, as it moved closer to the cyclone core. Then, around day 115 (June 9, 2004), the velocity quickly dropped when the radius was close to 15 km. On days 114 and 115, the drifter trajectory resembled a random walk, with small distances between measurements and sharp changes in direction. This stage is not visible on Figures 9-11 because of the small spatial extent of this random walk. Then, the ellipse radius and velocity experienced by the drifter quickly followed a Rankine-type profile, this time associated with a cyclone of lower intensity. The close-to-linear profile of the velocity with respect to the radius indicates this time a relative vorticity equal to $\zeta = 1.7 * 10^{-5}\ s^{-1}$, which is typical of low intensity cyclones observed in along-track altimetry. The Rankine-type profile estimated for the second cyclone is shown in Figure 11b.

This drifter trajectory is the first continuous observation dataset to document abrupt, intense changes experienced by a LCFE in the deep GoM. The analysis based on time-varying

ellipse decomposition provides a very useful insight into what was qualitatively observed on SST maps and in the drifter trajectory (Figure 9). From the start of the looping movement, in early April, to the end of May, the drifter first followed the strongest SST gradient before migrating toward the cyclone core. This migration took place not long before a decrease in the cyclone size observed on SST maps. During that period, the drifter sampled the same cyclone whose characteristics followed a Rankine profile. In early June, together with the shrinking of the cyclone noticed in SST, the drifter left that cyclone and was quickly trapped in a second, less intense one. Such a succession of events suggests the following scenario: the first cyclone, as it extended southwestward toward the Campeche Bank, was surrounded for most of its circumference by the meandering LC; at that time, its shape was elongated from southwest to northeast, and the cyclone was subject to intense shear from the LC surrounding it. That shear lead first to the erosion, then to the collapse of the cyclone structure; water parcels from that first cyclone, mixing with surrounding waters when the cyclone collapsed, had positive vorticity that was reduced compared to the initial cyclone. These parcels still managed to form a second cyclone further to the east. This sequence would explain how the drifter could leave one cyclone before being trapped in another one so quickly. The collapse of a similarly elongated LCFE was noticed in a modeling study of a LCE shedding sequence (Le Hénaff et al., 2012b) and needs to be further investigated, based on the results from observations presented here. Finally, such changes in cyclone size and vorticity, as those experienced by this specific drifter, might explain why the cyclones observed in the Dry Tortugas area from along-track altimetry do not have characteristics similar to those of the cyclones observed upstream along the LC in the deep GoM, if LCFEs usually experience comparable changes between the deep southeastern GoM and the Dry Tortugas area.

The analysis of this particular trajectory shows, for the first time, that frontal eddies in the eastern GoM can be considered to be in solid-body rotation close to their core. This justifies *a posteriori* the approach followed in our altimetry analysis for deriving the relative vorticity from the along-track signal (Appendix A). The analysis also shows that the first identified cyclone was not intensified between the deep northeastern GoM and the deep southeastern GoM. This suggests that the strong signal in altimetry-derived relative vorticity in the deep southeastern GoM area (Figure 3d) is due to the fact that only the most intense cyclones are advected from the deep northern GoM, and hence are selectively sampled; this feature is thus not due to actual eddy intensification. This new result complements previous findings related to the dynamics of LCFEs on the eastern side of the LC, although it needs to be confirmed by additional observations.

4.3 Evaluation of along-track altimetry results

The trajectory of drifter #40430 gives us the opportunity to evaluate results from the along-track altimetry analysis. Figure 12 shows various parameters estimated along the drifter trajectory by the along-track altimetry analysis. Figure 12a shows a map with the drifter trajectory, and all the cyclones detected by altimetry and associated with the LCFE sampled by drifter #40430 at the time of drifter observations. The various altimeters involved in the LCFEs detection are also indicated. All four altimeters in orbit in 2004 are used, which is very helpful to follow the LCFE and to perform the comparison with the drifter characteristics. This stresses the need for at least four altimeters in orbit to study mesoscale variability at regional scale (Pascual et al., 2006, 2007). Figure 12b shows the time evolution of the cyclones' diameter as observed by altimetry. Between days 40 and 80, the altimeters provide an estimate of the LCFE diameter in the 90 to 100 km range. Between day 80 and 115, when the LCFE migrated westward toward the

CB, the estimated diameter increases to 120 or 130 km diameter, after an estimate of 70 km around day 85. After the collapse of the first cyclone and the formation of the second one around day 115 (noted on Figure 12b-d), the second LCFE shows a wide range for the estimated diameter, between 110 and 160 km. We previously saw that shortly before the collapse of the first cyclone, its boundaries estimated by along-track altimetry were a little outside the strongest SST gradient. We also found that the southern boundary of the second cyclone estimated from altimetry was far south compared to the drifter trajectory. This indicates an overestimation of the cyclone size in the along-track altimetry signal around this location. Such an overestimation might be due to the influence of the LC, which was then surrounding the whole cyclone. At the end of the time series, the last two observed radii are more consistent, close to 100 km diameter.

Figure 12c shows the time series of the cyclones' amplitude. This amplitude was initially consistent, between 15 and 25 cm. It increased to very large values (around 35 cm) between day 80 and 115, during the migration and erosion of the first LCFE. After the collapse of the first cyclone and the formation of the second one, the amplitude shows values that are lower for the second LCFE than the initial values for the first one (between 10 and 15 cm). These estimates thus indicate that the amplitude of the second LCFE was slightly lower than the amplitude of the first one, although it is difficult to confirm that the signal is associated with two different cyclones based on that estimate only. Such a diagnostic is more obvious when based on the estimation of relative vorticity, shown in Figure 12d. The relative vorticity was quite large initially, with a wide range of values between 3.5 and 7.5 $*10^{-5}$ s^{-1} that were generally larger than the estimate from the time-varying ellipse decomposition of the drifter trajectory (which was 4.2 $*10^{-5}$ s^{-1}, indicated on Figure 12c), although the numbers are comparable. After day 115, the estimated relative vorticity from altimetry was between 1 and 2.5 $*10^{-5}$ s^{-1}, generally in close

agreement with the value estimated from the ellipse decomposition of the drifter trajectory, which was 1.7 $*10^{-5}$ s^{-1} (also indicated on Figure 12c). Contrary to the estimates of the eddy diameter and amplitude, it is clear from the relative vorticity estimates that they actually describe two distinct cyclones. Thus, relative vorticity appears to be the most robust quantity estimated in our along-track altimetry analysis (Section 2) to identify and analyze changes in eddy dynamics; this justifies *a posteriori* the choice to analyze this quantity in more detail.

5. Conclusion

We used two datasets to characterize the cyclonic activity in the eastern GoM, which is closely related to the Loop Current (LC) extension and LC Eddy (LCE) shedding. The first dataset is based on remotely sensed, along-track altimetry data, from 1992 to 2011. The second one is an *in situ* dataset based on the GDP near-surface drifters, from 1993 to 2011. From these unprecedented long datasets, and the detailed analysis of an especially long drifter trajectory, we were able to bring new insights and complement earlier findings regarding the characteristics of the cyclonic LC frontal eddies (LCFEs) in the Gulf of Mexico (GoM).

The new findings from this study are:

a) The analysis of the long drifter trajectory indicates that LCFEs have a Rankine profile; in particular, their core is in solid body rotation. This property, together with the hypothesis of geostrophy, allows for deriving the relative vorticity of LCFEs based on along-track altimetry data.

b) LCFEs observed in the deep southeastern GoM show intense relative vorticity, but they are not frequently observed. The analysis of the long drifter trajectory suggests that among the LCFEs in that area, those that have been advected from the northern GoM are not intensified along their way or locally, but have kept their original relative vorticity. In particular, this suggests that only LCFEs with intense relative vorticity are advected southward along the east of the LC, and can then play a role in LCE detachment or separation, as reported in previous studies (e.g. Vukovich and Maul, 1985; Schmitz, 2005).

c) LCFEs on the eastern Campeche Bank slope area are preferably found immediately after a LCE detachment or separation, based on altimetry. Since earlier studies found that these LCFEs are usually involved in a LCE shedding event (e.g. Zavala-Hidalgo et al., 2003), this result suggests that they can be involved in the shedding only after the subsequent re-attachment of the LCE. This result remains to be confirmed, as the analysis of altimetry data and drifter trajectories shows some discrepancies between the datasets.

In addition, this study presents, for the first time, quantitative evidence, derived from observations, of processes so far only identified with model simulations:

d) Based on both datasets, LCFEs flowing from the Mississippi Fan to the deep northeastern Gulf of Mexico (GoM) experience an intensification of their relative vorticity. The observed intensification is consistent, in location and intensity, with results from the model study of Le Hénaff et al. (2012b), who attributed this intensification to vortex stretching forced by the Mississippi Fan topography.

e) A small area just north of the Campeche Bank slope along the LC pathway at (88°W; 24.5°N) is associated with intense cyclones detected in relative vorticity derived from altimetry,

albeit less clearly in the drifter analysis. This area is consistent with the location of intense baroclinic instability noticed in a model simulation by Oey (2008). These cyclones seem to be associated with local LCE detachment or separation, also consistent with results of Oey (2008).

Finally, the ~20 year long datasets used in this study confirm or complement results from previous studies, which were based on single observations, or limited (in duration and/or quality) observation datasets:

f) Tortugas Eddies are the most frequently observed LCFEs in altimetry, but only when the LC extends beyond 25.5°N. They experience changes in their characteristics (diameter, amplitude, relative vorticity), estimated from altimetry, before or during their stay at their typical observed location (83.5°W; 24°N). This latter result complements findings from Fratantoni et al. (1998) and Kourafalou and Kang (2012), who studied the deformation of Tortugas Eddies under the influence of topography once they are advected into the Straits of Florida. We show in this study that modifications of Tortugas Eddies can also take place before they enter the Straits of Florida. The analysis of a single trajectory, together with SST maps, shows the collapse of an initially intense LCFE, followed by the formation of a second, less intense one, immediately upstream of the area where the Tortugas Eddies are observed. We suggest that the first cyclone was eroded by the intense shear due to the LC, which then surrounded the cyclone, and that the second one was formed from remnants of the first one. This mechanism possibly explains why Tortugas Eddies have different characteristics than cyclones observed upstream the LC.

g) Based on altimetry, the central eastern GoM is associated with large LCFEs detected in altimetry, but with rather weak relative vorticity. This area coincides with the location noticed by Zavala-Hidalgo et al. (2002) for large cyclones north of the LC that can block its extension for

long periods of time. Here it appears that occurrences of such large cyclones do not happen only during long separation intervals (when the LC stays unusually retracted before extending), as was previously commonly thought, but also during more standard LC extension phases, and even during temporary LCE detachments.

h) Based on altimetry, LCFEs have diameter values generally ranging from 80 to 120 km, in agreement with previous estimates (e.g. Vukovich and Maul, 1985), and tend to be of larger dimension in the northern and eastern side of the LC than on the western side, in agreement with Vukovich (1988).

i) LCFEs are statistically more frequently observed in the deep northeastern GoM than in any other portion of the LC edge (except in the vicinity of the Dry Tortugas), which indicates that they tend to stay blocked there. This result from the ~20 year long altimetry dataset is consistent with previous findings based on individual episodes, from Walker et al. (2011) using mapped altimetry and SST observations in spring 2010, or Le Hénaff et al. (2012b) examining a LCE shedding sequence from a model simulation.

In addition to these findings, which are specific to the GoM, this study also lead to improvements in the data treatment of both along-track altimetry data and surface drifter trajectories (presented in Appendices A and B):

j) The wavelet analysis of along-track altimetry data, based on the work by Dussurget et al. (2011), has been upgraded to include an estimation of eddy relative vorticity, in addition to the eddy center, amplitude and boundaries. This relative vorticity is consistent with the estimates from the drifter trajectory. Relative vorticity appears to be the most robust diagnostic for identifying and characterizing cyclones based on along-track altimetry data.

k) In order to keep valuable data from drifters after they lost their drogues, we implemented a selection of such drifter data when local winds have small amplitude. Such an approach is suitable in sub-tropical and tropical domains, where winds are expected to be of low intensity.

The combination of long datasets from both remote sensing and *in situ* observations is a powerful approach, both in a statistical sense and when comparisons during a specific event allow for evaluating the robustness of the diagnostics and complementing the initial results. This approach was very fruitful for deriving precise characteristics of the LC frontal dynamics. Altimetric data are especially useful when four altimeters are simultaneously in orbit, stressing the need for such a constellation to study regional mesoscale variability, as recommended from studies in other areas (e.g. in the Mediterranean Sea, Pascual et al., 2007). Finally, the use of along-track altimetry allows keeping the original sea surface height slopes at the mesoscale, hence deriving the LCFEs' relative vorticity quite accurately, which would not be possible with existing mapped products. This dataset gives very precise information in the dynamically and topographically complex GoM region. The approach followed in this study could certainly be applied in other areas, especially in regional domains with strong topographic constraints.

Acknowledgments

The along-track altimetric products were produced and distributed by Aviso (http://www.aviso.oceanobs.com/) as part of the Ssalto ground processing segment. The mapped altimetry products were produced by Ssalto/Duacs and distributed by Aviso, with the support from CNES (http://www.aviso.oceanobs.com/duacs). MDT_CNES-CLS09 was produced by CLS

Space Oceanography Division and distributed by Aviso, with the support from CNES (http://www.aviso.oceanobs.com/). Global Drifter Program data are distributed by NOAA (http://www.aoml.noaa.gov/phod/dac/index.php). The MUR Global High-Resolution SST dataset is distributed by NASA (http://podaac.jpl.nasa.gov/dataset/JPL-L4UHfnd-GLOB-MUR). The authors wish to thank Annalisa Griffa, Jonathan Lilly and Inga Koszalka for very fruitful discussions. They also thank two anonymous reviewers for their constructive remarks. Partial support for this study was provided by the National Science Foundation (NSF OCE-0929651) and the National Oceanic and Atmospheric Administration (NOAA NAI7RJ1226 and NA11NOS4780045). R. D. is supported by Ifremer through a post-doctoral fellowship, co-funded by Collecte Localisation Satellites (CLS, France). R. L. is supported by NOAA's Climate Program Office and the Atlantic Oceanographic and Meteorological Laboratory.

Appendix A: along-track altimetry data treatment

Along-track SSH data are analyzed based on wavelet decomposition. Wavelet analysis is based on the decomposition of the signal of interest into orthogonal, multi-resolution wave packets, in a similar way to Fourier decomposition. This approach allows for the detection of spectral characteristics of non-stationary processes in both time and space (Torrence and Compo, 1998). Here, we perform a wavelet analysis on altimetry-derived SSH data, in search of the signature of the passage of eddy-like structure along each satellite track. This approach has proven to be robust for analyzing mesoscale eddies in the Labrador Sea (Lilly et al., 2003), and in the Bay of Biscay (Dussurget et al., 2011).

We assume that the along-track SSH signature of the Loop Current Frontal Eddies (LCFEs) have Gaussian properties, as was assumed for mesoscale eddies in the Bay of Biscay (Dussurget et al., 2011). We use a wavelet function from the class of Derivative Of a Gaussian (DOG) functions (with $m = 0$, i.e. the function is a pure Gaussian) to analyze the along-track SSH data in the search of eddy signature (Torrence and Compo, 1998).

If we consider a series of successive along-track SSH x_n, and our wavelet function ψ (here the real-valued Gaussian function), then the wavelet transform of x_n by ψ is:

$$W_n(s) = \frac{1}{N}\sum_{k=0}^{N-1} \hat{x}_n * \hat{\psi}(s\omega_k) e^{i\omega_k n \delta t} \qquad \text{[A1]}$$

where N is the number of points in the satellite track, δt is the along-track resolution (~6 km), and ω_k is the angular frequency (in space):

$$\omega_k = \begin{cases} \frac{2\pi k}{N\delta t} : k \le \frac{N}{2} \\ -\frac{2\pi k}{N\delta t} : k > \frac{N}{2} \end{cases} \qquad \text{[A3]}$$

$\hat{x}_n$ is the discrete Fourier transform of the SSH series:

$$\hat{x}_n = \frac{1}{N}\sum_{k=0}^{N-1} x_n * e^{-2\pi i k n / N} \qquad \text{[A4]}$$

In the case of a Gaussian function, the wavelet ψ and $\hat{\psi}$, its discrete Fourier transform, are of the form (Torrence and Compo, 1998):

$$\psi(\eta) = \frac{(-1)}{\sqrt{\Gamma(1/2)}} \frac{d}{d\eta}\left(e^{-\eta^2/2}\right) \quad [A5]$$

$$\hat{\psi}(s\omega) = \frac{1}{\sqrt{\Gamma(1/2)}} (s\omega) e^{-(s\omega)^2/2} \quad [A6]$$

The wavelet analysis performed here searches for local maxima in the wavelet energy, i.e. when the convolution of ψ with x_n reaches a maximum, which happens when a Gaussian feature is present in the along-track SSH. An example of a wavelet function used to identify the maximum wavelet energy when convoluted with SSH series can be seen in Dussurget et al. (2011, their Figure 6). We select a range of wavelengths, from j_1 to j_2, between which we estimate a scale-averaged spectrum of x_n:

$$\bar{W}_n = \frac{\delta j \delta t}{C_\delta} \sum_{j=j_1}^{j_2} \frac{\left|W_n(s_j)\right|^2}{s_j} \quad [A7]$$

where δj is the scale interval, $s_j = s_0 2^{j\delta j}$, with s_0 the smallest resolvable scale (approximately $2\delta t$), and C_δ is a reconstruction factor, specific to the wavelet function. For the Gaussian function used here, C_δ = 7.011324 (estimated by Monte-Carlo method, Dussurget, pers. comm.). The lower and upper indexes j_1 and j_2 are chosen so that the corresponding spatial scales are 40 and 1000 km. The value of 40 km allows filtering out small-scale signal while keeping the dominant signal associated with the LCFEs, which are expected to have typical dimension of 80 to 120 km (Vukovich and Maul, 1985). The upper boundary is chosen large in order to consider all scales above 40 km. A local maximum of the scale-averaged spectrum indicates the location of the central position of an eddy along the satellite track. In this study, only peaks of amplitude $\sqrt{\bar{W}_n}$ larger than 5 cm are considered to be associated with eddies. Also, we only study eddies

corresponding to a local SSH low, in order to select only cyclonic eddies. These include the LCFEs we are interested in.

The wavelet decomposition is also used as a way to smooth the along-track SSH signal, using the filtering methodology described in Torrence and Campo (1998). The smoothed signal is reconstructed as the sum of the various wavelet components, between the selected wavelengths:

$$x_n = \frac{\delta j \delta t^{1/2}}{C_\delta \psi_0(0)} \sum_{j=j_1}^{j_2} \frac{W_n(s_j)}{s_j^{1/2}} \qquad \text{[A8]}$$

The smoothed SSH is then used to derive the across-track geostrophic surface current, using the approach by Powell and Leben (2004). The smoothing of the SSH signal is necessary because the geostrophic current is proportional to the first derivative of SSH in space, and as such is very sensitive to small scale SSH variations, which are often considered as noise in the observations. Through geostrophy, this current is perpendicular to the direction of the track. The geostrophic current is used to determine the boundaries of the eddy, considered to be the closest local maxima in current intensity on each side of the eddy center previously estimated. These boundaries allow us to calculate the diameter of the eddy. The amplitude of the eddy is then calculated as the difference between the smoothed SSH at the center of the eddy and the average value of the smoothed SSH at the eddy boundaries. Note that these estimates of the eddy size and amplitude slightly differ from the method employed by Dussurget et al. (2011), who estimated these values directly from the scale-averaged spectrum. The method proposed here appeared more robust in our study zone, based on thorough examination of several study cases.

Finally, the geostrophic surface current is used to estimate the surface relative vorticity inside the eddy. We consider that the eddy is geostrophic and in solid-body rotation close to its center. Hence, in the core of the eddy, the relative vorticity is:

$$\zeta = v_g / r \qquad \text{[A9]}$$

where v_g is the azimuthal geostrophic current, estimated from the along-track SSH, and r the distance from the eddy center. We use the mean value of v_g/r close to the eddy core to estimate the relative vorticity associated with each eddy, with r smaller than the typical Rossby radius of deformation (which is about 30 km in the Gulf of Mexico; Oey et al., 2005). For eddies with radius smaller than the Rossby radius of deformation, r is taken smaller than the distance between the cyclone center and the associated boundary, as estimated by the geostrophic current field. The eddy relative vorticity is an additional eddy characteristic estimated for our study, compared to Dussurget et al. (2011).

The estimation of the relative vorticity presented here is valid only if the estimated center of the eddy is close to the actual center of the eddy, and if the eddy has a symmetric structure with respect to its center. While the first criterion is impossible to verify without independent observations, we make sure that we consider eddies that reasonably respect the second criterion. To do so, we discard eddies for which the distance between the center and the closest boundary is less than 0.3 times the distance between the center and the furthest boundary. While this number is quite small compared to 1 (full symmetry), this leads to discarding about 13.3% of the dataset.

Finally, we define a Euclidean norm for each eddy, estimated from the normalized values of the eddy diameter, amplitude and relative vorticity. We only keep data below the 95th percentile estimated from the value of that norm for all the cyclones in the dataset, in order to

discard large outliers that might dominate the mean values, while keeping a large number of individual observations in the dataset. After these various filtering steps, the total number of individual cyclone observations in along-track profiles in the eastern GoM is 4252 in our dataset.

Note that the codes used to perform the wavelet analysis presented here are freely available[1].

Appendix B: Compilation of an extended drifter data set for the GoM

The GDP data are sensitive to potential drogue losses, which can severely affect their motion in the presence of high winds (Grodsky et al., 2011). Indeed, if the drifter loses its drogue, it becomes very sensitive to the direct wind effect on the surface spherical buoy. It is thus common to discard all data from drifters once they have lost their drogue. This is a very safe approach, particularly in areas where winds are especially intense, like the Southern Ocean (Grodsky et al., 2011). However, this might not be necessary in areas where the surface winds are usually of low amplitude, typically in subtropical domains like the GoM. Figure B1 shows three trajectories from the GDP dataset, for which the drifter lost its drogue quite early in its lifetime. Figure B1a shows the trajectory of one of the 40 SVP drifters deployed in response to the Deepwater Horizon oil spill. The drifter was deployed along the continental slope north of the CB on July 13, 2010 (in dark blue). It was first entrained southeastward, and lost its drogue after only 5 days. In spite of this, after the drogue loss the drifter was clearly entrained by the clockwise cyclone that then stood between the retracted LC and the detached LC Eddy "Franklin". The drifter was then entrained westward in another cyclonic loop on the CB slope, before being

[1] https://code.google.com/p/py-altiwaves/

entrained in four anticyclonic loops around Eddy Franklin. Finally, it was entrained by the LC toward the Straits of Florida. It is clear that this trajectory provides relevant physical information about the GoM circulation despite the loss of the drifter drogue.

The second example of such trajectory also comes from a drifter deployed in response to the Deepwater Horizon oil spill (Figure B1c). The drifter was deployed on July 17, 2010, this time on the slope along the northern GoM. It was first entrained southeastward toward the deep northeastern GoM, where it experienced a clockwise semi-rotation that brought it along the northern GoM shelf slope. The drifter followed this slope westward until 90°W, before turning southward. There, the drifter stayed in a small area on the shelf slope for a few days, during which time the drifter lost its drogue, 73 days after deployment. Following the loss of the drogue, the drifter was advected southward in the deep GoM, where it was entrained by Eddy Franklin during two loops. Then, it was stuck over the Mississippi Fan for a few weeks, before reaching the deep northern GoM and the edge of the West Florida Shelf. It then followed the shelf slope to the south, before being entrained in a cyclonic loop in the deep southeastern GoM. Finally, it was entrained by the LC toward the Straits of Florida. As noted previously, in spite of the drogue loss, the drifter was able to provide useful information on the GoM circulation. In particular, the drifter sampled Eddy Franklin, and was trapped by a potential LCFE on its way out of the GoM.

A final example trajectory comes from a drifter released in 2003 outside the GoM, which was advected through the Yucatan Channel (Figure B1e). The drifter was clearly entrained initially by the LC along the edge of CB toward the northern GoM. It lost its drogue while in the deep part north of the CB. Later, it was advected by the LC over the Mississippi Fan and reached the deep northeastern GoM, where it was trapped by a cyclonic eddy. It kept a cyclonic motion all along the eastern GoM, along the West Florida Shelf, before being entrained outside the GoM

by the exiting LC. It is obvious that such a trajectory provides very useful information on the LCFE dynamics, and the corresponding data should be kept for such purpose.

It thus appears that many of the drifter measurements made after drogue loss are still useful for the study of the GoM dynamics and should be kept in the drifter dataset. Pazan and Niiler (2001) studied the differences in behavior of drifters with and without their drogues on, in order to recover consistent data from undrogued drifters. In particular, they estimated that the amplitude of the difference in velocities between SVP drifters with and without drogue was $7.9*10^{-3}$ W, where W is the surface wind amplitude. We thus compared the drifter velocities to this quantity for the trajectories shown on Figures B1a,c,e, along each drifter trajectory inside the GoM (Figures B1b,d,f). The drifter whose trajectory is shown on Figure B1a shows a quite small value of the ratio $7.9*10^{-3}$ W/U (Figure B1b), even after the drifter lost its drogue, which indicates that the undrogued drifter trajectory is close to the one it would have, had it still had its drogue on. This is consistent with the observation that the drifter was following ocean features, such as LCE Franklin and a LCFE. The second drifter, shown on Figure B1c, shows larger values for the ratio $7.9*10^{-3}$ W/U (Figure B1d). Values larger than 1 indicate that the expected difference between the observed velocity from the undrogued drifter and the velocity that the drifter would have if drogued is larger than the observed velocity itself, so that the influence of the wind on the trajectory is expected to be large. For drifter #98940 (Figures B1c,d), such large values are reached around day 150, in a period during which the drifter was floating over the Mississippi Fan, first northward, then southeastward; such a trajectory cannot be clearly related to typical coastal ocean dynamics, as currents are usually aligned with the bathymetry contours. However, earlier than day 150 the value of the ratio was small, when the undrogued drifter was clearly following LCE Franklin (between day 75 and day 100). After day 150, the ratio dropped

significantly; during that period, the drifter was clearly trapped in a cyclone along the West Florida Shelf (around day 200). Finally, the third drifter presented on Figure B1e shows small values for the ratio $7.9*10^{-3}$ W/U after the drifter lost its drogue, with only isolated peaks of values reaching 1 or more (Figure B1f). The trajectory of that drifter clearly indicates it is trapped in a LCFE.

Based on this analysis, we defined a threshold value of 0.3 for the ratio $7.9*10^{-3}$ W/U, above which the drifter observations should be discarded. This threshold value of 0.3 is indicated on Figures B1b,d,f with a dashed line. This value allows keeping observations for periods when the drifters are associated with ocean processes, while discarding observations from periods when the wind dominates the drifter motion and ocean influence is more questionable.

References

Athié, G., Candela, J., Ochoa, J., Sheinbaum, J., 2012. Impact of Caribbean cyclones on the detachment of Loop Current anticyclones. J. Geophys. Res., 117, C03018, doi:10.1029/2011JC007090.

Borgas, M. S., Flesch, T. K., Sawford, B. L., 1997. Turbulent dispersion with broken reflectional symmetry. J. Fluid Mech., 279, 69-99.

Castelão G. P., Johns W. E., 2011. Sea surface structure of North Brazil Current ring derived from shipboard and moored acoustic Doppler current profiler observations. J Geophys. Res. 116:C01010. doi: 10.1029/2010JC006575.

Chérubin L. M., Morel, Y., Chassignet, E. P., 2006. Loop current ring shedding: the formation of cyclones and the effect of topography. J. Phys. Oceanogr. 36, 569–591.

Cochrane, J. D., 1972. Separation of an anticyclone and subsequent developments in the Loop Current (1969). In: Capurro, L. R. A., Reid, J. L. (Eds.), Contributions on the Physical Oceanography of the Gulf of Mexico. Gulf Publ. Co., Houston, Tex., pp. 91–106.

Dussurget, R., Birol, F., Morrow, R., De Mey, P., 2011. Fine resolution altimetry data for a regional application in the Bay of Biscay. Mar. Geod. 34 (3–4), 447–476.

Flament, P. J., Lumpkin, R., Tournadre, J., Kloosterziel, R., Armi, L., 2001. Vortex pairing in an unstable anticyclonic shear flow: discrete subharmonics of one pendulum day. J. Fluid Mech., 440, 401–409.

Fratantoni, P. S., Lee, T. N., Podesta, G. P., Muller-Karger, F., 1998. The influence of loop current perturbations on the formation and evolution of Tortugas eddies in the southern Straits of Florida. J. Geophys. Res., 103(C11), 24759– 24779.

Griffa, A., Lumpkin, R., Veneziani, M., 2008. Cyclonic and anticyclonic motion in the upper ocean. Geophys. Res. Lett., 35, L01608, doi:10.1029/2007GL032100.

Grodsky, S. A., Lumpkin, R., Carton, J. A., 2011. Spurious trends in global surface drifter currents. Geophys. Res. Lett., 38, L10606, doi:10.1029/2011GL047393.

Ichiye, T., 1962. Circulation and water mass distribution in the Gulf of Mexico. Geofisica International (Mexico City) 2**,** 47–76.

Koszalka, I. M., LaCasce, J. H., 2010. Lagrangian analysis by clustering. Ocean Dyn., 60(4), 957-972.

Kourafalou, V. H., Kang, H., 2012. Florida Current meandering and evolution of cyclonic eddies along the Florida Keys Reef Tract: Are they interconnected? J. Geophys. Res., 117, C05028, doi:10.1029/2011JC007383.

LaCasce, J. H., Ohlmann, J. C., 2003. Relative dispersion at the surface of the Gulf of Mexico. J. Mar. Res., 61,285–312.

Larnicol, G., Mertz, F. , Rosmorduc, R., Delamarche, A. 2011. Product User Manual For Sea Level SLA Products version 2.1, MyOcean, (http://catalogue.myocean.eu.org/static/resources/myocean/pum/MYO-SL-PUM-008-001-to-005-v2.1.pdf).

Leben, R. R., 2005. Altimeter-derived loop current metrics. In: Sturges, W., Lugo-Fernandez, A. (Eds.), Circulation in the Gulf of Mexico: Observations and Models. American Geophysical Union, Washington, D. C., pp. 181–201.

Le Hénaff, M., Kourafalou, V. H., Paris, C. B., Helgers, J., Aman, Z. M., Hogan, P. J., Srinivasan, A., 2012a. Surface Evolution of the Deepwater Horizon Oil Spill Patch: Combined Effects of Circulation and Wind-Induced Drift. Environ. Sci. Technol., 46, 7267−7273.

Le Hénaff, M., Kourafalou, V. H., Morel, Y., Srinivasan, A., 2012b. Simulating the dynamics and intensification of cyclonic Loop Current Frontal Eddies in the Gulf of Mexico. J. Geophys. Res., 117, C02034, doi:10.1029/2011JC007279.

Le Traon, P.-Y., Nadal, F., Ducet, N., 1998. An Improved Mapping Method of Multisatellite Altimeter Data. J. Atmos. Oceanic Technol., 15, 522-534.

Le Traon, P.-Y., Morrow, R., 2001. Ocean currents and eddies. In: Cazenave , A., Fu, L.-L. (Eds.), Satellite Altimetry and Earth Sciences, Academic, San Diego, Calif., pp. 175 – 215.

Lee, T.N. and E. Williams, 1999. Mean distribution and seasonal variability of coastal currents and temperature in the Florida Keys with implications on larval recruitment. Bulletin of Marrine Science, 64(1), 35-56.

Lilly, J. M., Rhines, P. B., 2002. Coherent eddies in the Labrador Sea observed from a mooring. J. Phys. Oceanogr. 32 (2), 585–598.

Lilly, J. M., Rhines, P. B., Schott, F., Lavender, K., Lazier, J., Send, U., D'Asaro, E. 2003. Observations of the Labrador Sea eddy field. Prog. Oceanogr., 59(1), 75-176, doi:10.1016/j.pocean.2003.08.013.

Lilly, J. M., Scott, R. K., Olhede, S. C., 2011. Extracting waves and vortices from Lagrangian trajectories. Geophys. Res. Lett., 38, L23605, doi:10.1029/2011GL049727.

Lugo-Fernandez, A., Leben, R. R., 2010. On the linear relationship between Loop Current retreat latitude and eddy separation period. J. Phys. Oceanogr., 40, 2778-2784.

Lumpkin, R., Pazos, M., 2007. Measuring surface currents with Surface Velocity Program drifters: The instrument, its data, and some recent results. In: Griffa, A., et al., (Eds.), Lagrangian Analysis and Prediction of Coastal and Ocean Dynamics. Cambridge Univ. Press, Cambridge, U. K., pp. 39-67.

Lumpkin, R., Elipot, S., 2010. Surface drifter pair spreading in the North Atlantic. J. Geophys. Res., 115, C12017, doi:10.1029/2010JC006338.

Lumpkin, R., Grodsky, S., Rio, M.-H., Centurioni, L., Carton, J., Lee, D., 2013. Removing spurious low-frequency variability in surface drifter velocities. J. Atmos. Oceanic Technol., 30 (2), 353—360, doi:10.1175/JTECH-D-12-00139.1.

Morrow, R., Le Traon, P.-Y., 2011. Recent advances in observing mesoscale ocean dynamics with satellite altimetry. Journal of Advances in Space Research. http://dx.doi.org/10.1016/j.asr.2011.09.03.

Niiler, P. P., Paduan, J. D., 1995. Wind‐driven motions in the northeast Pacific as measured by Lagrangian drifters. J. Phys. Oceanogr., 25, 2819–2830.

Oey, L-Y., Ezer, T., Lee, H.-C., 2005. Loop Current, rings and related circulation in the Gulf of Mexico: A review of numerical models and future challenges. In: Sturges, W., Lugo-

Fernandez, A. (Eds.), Circulation in the Gulf of Mexico: Observations and Models. American Geophysical Union, Washington, D. C., pp 32-56.

Oey, L-Y., 2008. Loop Current and Deep Eddies. J. Phys. Oceanogr., 38, 1426-1449.

Ohlmann, J. C., Niiler, P. P., 2005. Circulation over the continental shelf in the northern Gulf of Mexico. Prog. .Oc., 64, 45–81.

Paillet, J., Le Cann, B., Carton, X. J., Morel, Y., Serpette, A., 2002. Dynamics and evolution of a northern meddy. J. Phys. Oceanogr., 32, 55– 79.

Paris, C. B., Cowen, R. K., Claro, R., Lindeman, K. C., 2005. Larval transport pathways from Cuban spawning aggregations (Snappers; Lutjanidae) based on biophysical modeling. Marine Ecology Progress Series, 296, 93-106.

Pascual, A., Faugère, Y., Larnicol, G., Le Traon, P.-Y., 2006. Improved description of the ocean mesoscale variability by combining four satellite altimeters. Geophys. Res. Lett., L0261:1-4, doi: 200610.1029/2005GL024633.

Pascual, A., Pujol, M. I., Larnicol, G., Le Traon, P.-Y., Rio, M.-H., 2007. Mesoscale mapping capabilities of multisatellite altimeter missions: First results with real data in the Mediterranean Sea. J. Mar. Syst., 65(1-4):190-211, doi: 10.1016/j.jmarsys.2004.12.004.

Pazan, S. E., Niiler, P. P., 2001. Recovery of near surface velocity from undrogued drifters. J. Atmos. Oceanic Technol., 18, 476-489.

Powell, B. S., Leben, R. R., 2004. An optimal filter for geostrophic mesoscale currents from along-track satellite altimetry. J. Atmos. Oceanic Technol., 21, 1633-1642.

Reverdin, G., Niiler, P. P., Valdimarsson, H., 2003. North Atlantic Ocean surface currents. J. Geophys. Res., 108(C1), 3002, doi:10.1029/2001JC001020.

Richardson, P. L., 1993. A census of eddies observed in North Atlantic SOFAR float data. Prog. Oceanogr., 31, 1-50.

Rio, M.-H., Guinehut, S., Larnicol, G., 2011. New CNES-CLS09 global mean dynamic topography computed from the combination of GRACE data, altimetry, and in situ measurements. J. Geophys. Res., 116, C07018,doi:10.1029/2010JC006505.

Schmitz, W. J., 2003. On the circulation in and around the Gulf of Mexico (http://www.serf.tamus.edu/gomcirculation).

Schmitz, W. J., 2005. Cyclones and westward propagation in the shedding of anticyclonic rings from the Loop Current. In: Sturges, W., Lugo-Fernandez, A. (Eds.), Circulation in the Gulf of Mexico: Observations and Models. American Geophysical Union, Washington, D. C., pp 241-261.

Tester, P. A., Stumpf, R. P., Vukovich, F. M., Fowler, P. K., Turner, J. T., 1991. An expatriate red tide bloom: transport, distribution, and persistence. Limnol. Oceanogr., 36(5), 1053-1061.

Torrence, C., Compo, G. P., 1998. A practical guide to wavelet analysis. Bull. Am. Meteorol. Soc., 79(1), 61-78.

Veneziani, M., Griffa, A., Reynolds, A. M., Mariano, A. J., 2004. Oceanic turbulence and stochastic models from subsurface Lagrangian data for the Northwest Atlantic Ocean. J. Phys. Oceanogr., 34, 1884-1906.

Veneziani, M., Griffa, A., Garraffo, Z. D., Chassignet, E. P., 2005. Lagrangian spin parameter and coherent structures from trajectories released in a high-resolution ocean model. J. Mar. Res., 63, 753-788.

Vukovich, F. M., 1988. Loop Current boundary variation. J. Geophys. Res. 93, 585–615.

Vukovich, F. M., Maul, G. A., 1985. Cyclonic eddies in the eastern Gulf of Mexico. J. Phys. Oceanogr., 15, 105–117.

Walker, N. D., Leben, R. R., Anderson, S., Feeney, J., Coholan, P., Sharma, N., 2009. Loop Current frontal eddies based on satellite remote sensing and drifter data. OCS Study MMS 2009-023. U.S. Dept. of the Interior, Minerals Management Service, Gulf of Mexico OCS Region.

Walker, N. D., Pilley, C. T., Raghunathan, V. V., D'Sa, E. J., Leben, R. R., Hoffmann, N. G., Brickley, P. J., Coholan, P. D., Sharma, N., Graber, H. C., Turner, R. E., 2011. Loop Current Cyclonic Eddy Merger Impacts BP Gulf Oil Spill. In: Liu, Y., MacFadyen, A., Ji, Z.-G., Weisberg, R. H. (Eds.), Monitoring and Modeling the Deepwater Horizon Oil Spill: A Record-Breaking Enterprise. American Geophysical Union, Washington, D. C., pp 103-116.

Zavala-Hidalgo J., Morey, S. L., O'Brien, J. J., 2002. On the formation and interaction of cyclonic eddies with the Loop Current using NCOM and a suite of observations. In: Proceedings of the Oceans 2002 MTS/IEEE Conference, IEEE Catalog Num. 02CH37362C, 1463-1466.

Zavala-Hidalgo, J., Morey, S. L., O'Brien, J. J., 2003. Cyclonic eddies northeast of the Campeche Bank from altimetry data. J. Phys. Oceanogr., 33, 623– 629.

Zavala-Hidalgo, J., Morey, S. L., O'Brien, J. J., Zamudio, L., 2006. On the Loop Current eddy shedding variability. Atmosfera, 19(1), 41–48

Figure captions

Figure 1. Topography of the Gulf of Mexico (m), with various stages of the Loop Current extension: retracted, or port-to-port (purple), average extended position (green), and fully extended with a LC Eddy shed (red). Adapted from Le Hénaff et al. (2012) and based on Schmitz (2003), with values updated from Leben (2005) for the minimum, average and maximum meridional extension. Important bathymetric or geographic features are noted: the Campeche Bank, the West Florida Shelf, the Yucatan Channel (YC), the Mississippi Fan (MF) and the area near the Dry Tortugas (DT), where Tortugas Eddies were observed by Fratantoni et al. (1998).

Figure 2. Altimeter tracks used for studying cyclones in the eastern Gulf of Mexico. Five altimeters are used: Topex/Poseidon (TP), Jason-1 (J1), Jason-2 (J2), Envisat and GFO. In blue are the reference tracks from TP, J1 and J2; in red are the TP and J1 tracks on the interleave orbit; in green are the Envisat tracks; in orange are the GFO tracks. Isobaths of 200 m, 2000 m, and 3000 m are plotted in thin black lines.

Figure 3. Maps of the average cyclone characteristics estimated from along-track altimetry, on a 1/3° grid: (a) observation frequency (% of satellite passes); (b) diameter (km); (c) amplitude (cm); (d) relative vorticicty (10^{-5} s^{-1}); (e) distance to the LC or an LCE along the track (km). See text for the details on the estimation of the various quantities. Isobaths of 200 m, 2000 m, and 3000 m are plotted in thin black lines. A typical extended LC pathway, adapted from

Vukovich (1988), is added (thick red line). Various zones of interest (see Figure 4) are indicated by thin magenta lines.

Figure 4. Map showing various areas of interest, used for deriving distributions of certain cyclone characteristics. The various zones are: the Mississippi Fan (MF, orange); the deep northeastern GoM (dNEG, solid blue); the deep eastern GoM (dEG, green); the deep southeastern GoM (dSEG, solid red); the deep central GoM (dCG, yellow); the Dry Tortugas (DT, magenta); the northern Campeche Bank (NCB, dashed red); the eastern Campeche Bank (ECB, dashed blue). Isobaths of 200 m, 2000 m, and 3000 m are plotted in thin black lines.

Figure 5. Normalized distribution of the LC northern extension at the time of cyclone detection (color-filled histograms, degrees of latitude, 23.0 – 28.5°N), for the eight regions of interest (see Figure 4). The LC northern extension is estimated from mapped AVISO SSH data (see text for more details). In color is the associated relative vorticity (10^{-5} s^{-1}). The reference distribution of the LC northern extension at all times is added in each subplot (histograms with thin black contours). Colors underlining each area name reference the colors used for that area in Figure 4.

Figure 6. Trajectories of the 148 GDP drifters advected inside the GoM, from 1993 to 2011. Isobaths of 200 m, 2000 m, and 3000 m are plotted in thin black lines.

Figure 7. Time series of the daily number of drifter observations inside the GoM, for each year from 1993 to 2011 (x-axis). In red are the values when considering data only if the drifter's drogue is on; in blue are the values from the extended dataset (see Appendix B). The total number of observations in each case is indicated in the panel.

Figure 8. Average spin (Ω, 10^{-6} s^{-1}) estimated in the eastern GoM from the drifter trajectories. Patches of $\Omega>0$ denote cyclonic motion; patches with $\Omega<0$ denote anticyclonic motion. (a) All data before April 2010 are considered; (b) All data from 1993 to 2011 are considered; (c) All data before April 2010 are considered, with the exception of drifter #40430 (see Figure B1e).) Isobaths of 200 m, 2000 m, and 3000 m are plotted in thin black lines. The grid corresponding to various domains of interest defined in Figure 4 is added (thin magenta lines).

Figure 9. SST (°C) maps from the GHRSST-MUR dataset, with daily data at 0.011° resolution. The trajectory of drifter #40430 up to the SST observation date is depicted (blue line), with the locations of observations at the exact same date (blue points circled in black). The satellite track from one of the four altimeters in orbit, which detects a cyclone in the same area and same date (+/- 1 day) as the drifter looping, is added (thick black line), with the estimated center of the corresponding cyclone (magenta point circled in black), and the estimated cyclone boundaries (green points circled in black). The dates considered are: (a) April 8, 2004; (b) April

21, 2004; (c) May 3rd, 2004; (d) May 18, 2004; (e) May 28, 2004; (f) June 23, 2004. The grid corresponding to various domains of interest defined in Figure 4 is added (thin green lines). Isobaths of 200 m, 2000 m, and 3000 m are plotted in thin black lines.

Figure 10. Decomposition of drifter #40430 trajectory in a geometric grid (km): reference trajectory (black), some of the ellipses estimated from the trajectory decomposition technique by Lilly et al. (2011, blue), residual (red).

Figure 11. Focus on the elliptical part of the decomposition of drifter #40430 trajectory: (a) trajectory of the drifter (magenta line), with the locations and days (days since February 15, 2004) of individual observations corresponding to an elliptical motion as identified by the decomposition of the trajectory; the grid corresponding to various domains of interest defined in Figure 4 is added (thin blue lines); (b) Values of velocities (y-axis, $cm.s^{-1}$) vs. radius (x-axis, km), for each observation location shown in (a); (b) black lines denote estimated velocity profiles for Rankine-type cyclones approximately fitting the observed velocity-radius profiles (see text for more details).

Figure 12. (a) Trajectory of drifter #40430 (magenta), with the individual altimetry observations of a cyclone at the location and date (+/- 1 day) of a drifter's loop (colored point circled in black, blue: Jason 1, red: Topex/Poseidon, green: Envisat, orange: GFO); (b) individual estimations of the cyclone diameter (km) from along-track altimetry, along the drifter trajectory (days since February 15, 2004); (c) same as (b), for the cyclone amplitude (cm); (d) same as (b) for the cyclone relative vorticity (10^{-5} s^{-1}); the two values estimated from the drifter trajectory decomposition are added for day 40 to day 115, and from day 115 to day 160, as a reference (dashed lines). (b-d) The collapse of the first eddy on day 115 (June 9, 2004) is added (vertical dashed black line).

Figure B1. (a,c,e) Individual trajectories of three drifters, with associated age in the study area (in days). Each drifter identification number, initial and final dates in the area noted on Figure 6 are indicated in the title. Isobaths of 200 m, 2000 m, and 3000 m are plotted in thin black lines. (b,d,f) Time series (in days) of the ratio 0.0079*W/U, where W is the amplitude of the surface wind, and U the amplitude of the drifter velocity, for the three drifter trajectories; in blue is the period along the trajectory when the drifter's drogue is on, in red is the part when the drogue is off, and in black is the period when the drogue is off, low-pass filtered using a 5-day Loess filter; the mean value of the ratio for the period when the drogue is off is indicated in each panel; the value 0.3 is added on each panel (dashed black line), as a comparison.

Figures

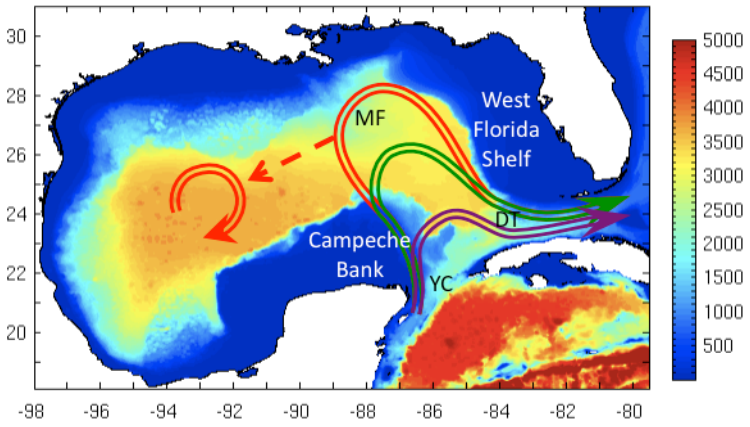

Figure 1. Topography of the Gulf of Mexico (m), with various stages of the Loop Current extension: retracted, or port-to-port (purple), average extended position (green), and fully extended with a LC Eddy shed (red). Adapted from Le Hénaff et al. (2012) and based on Schmitz (2003), with values updated from Leben (2005) for the minimum, average and maximum meridional extension. Important bathymetric or geographic features are noted: the Campeche Bank, the West Florida Shelf, the Yucatan Channel (YC), the Mississippi Fan (MF) and the area near the Dry Tortugas (DT), where Tortugas Eddies were observed by Fratantoni et al. (1998).

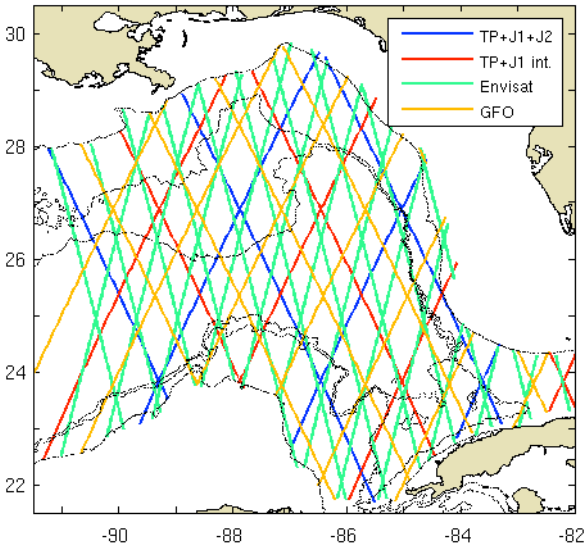

Figure 2. Altimeter tracks used for studying cyclones in the eastern Gulf of Mexico. Five altimeters are used: Topex/Poseidon (TP), Jason-1 (J1), Jason-2 (J2), Envisat and GFO. In blue are the reference tracks from TP, J1 and J2; in red are the TP and J1 tracks on the interleave orbit; in green are the Envisat tracks; in orange are the GFO tracks. Isobaths of 200 m, 2000 m, and 3000 m are plotted in thin black lines.

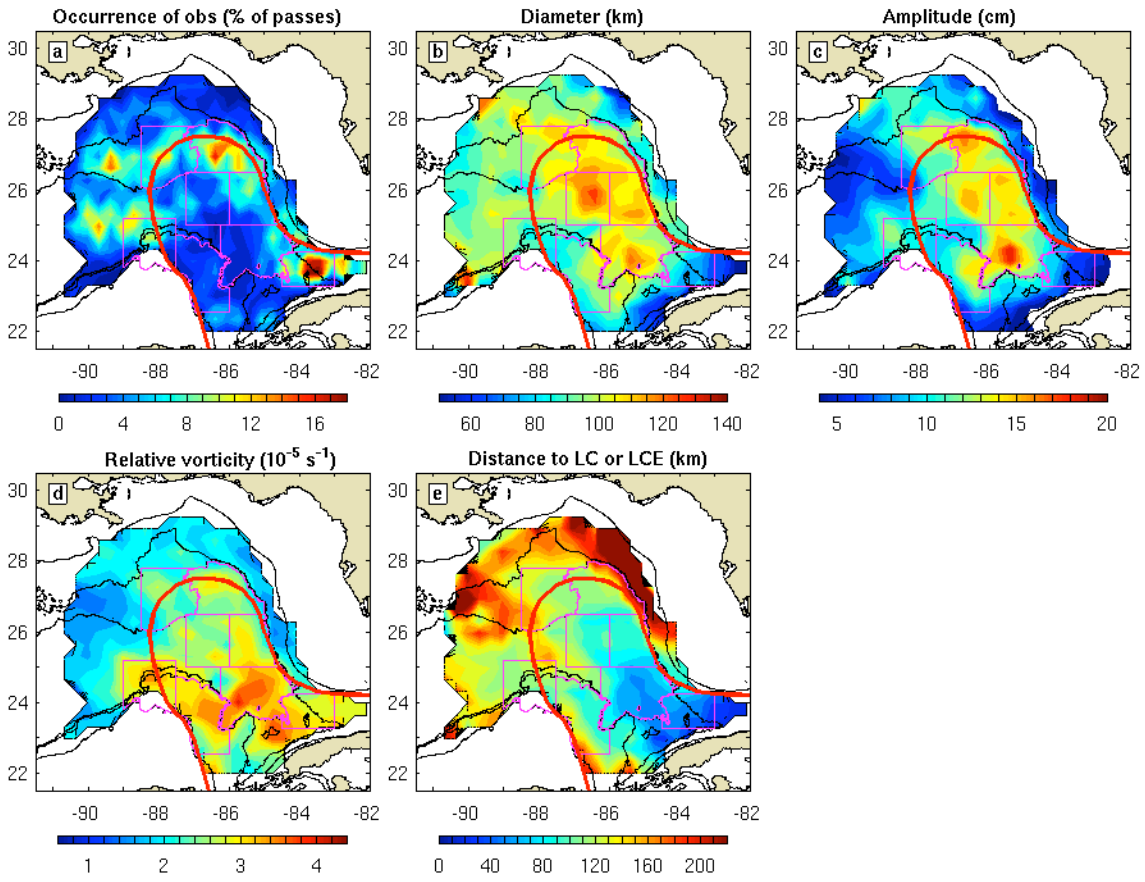

Figure 3. Maps of the average cyclone characteristics estimated from along-track altimetry, on a 1/3° grid: (a) observation frequency (% of satellite passes); (b) diameter (km); (c) amplitude (cm); (d) relative vorticicty (10^{-5} s^{-1}); (e) distance to the LC or an LCE along the track (km). See text for the details on the estimation of the various quantities. Isobaths of 200 m, 2000 m, and 3000 m are plotted in thin black lines. A typical extended LC pathway, adapted from Vukovich (1988), is added (thick red line). Various zones of interest (see Figure 4) are indicated by thin magenta lines.

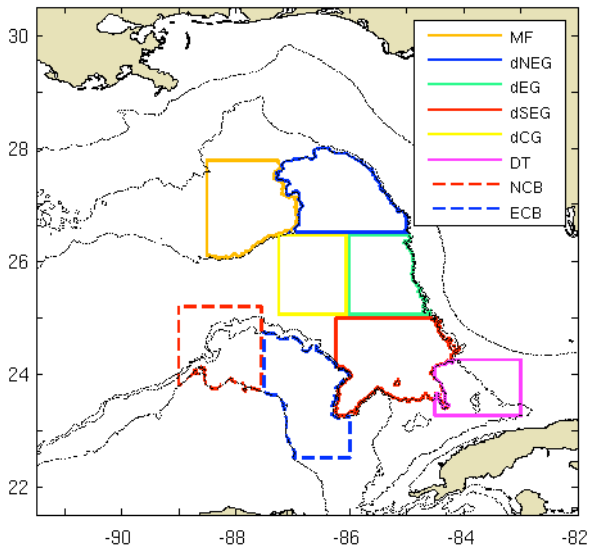

Figure 4. Map showing various areas of interest, used for deriving distributions of certain cyclone characteristics. The various zones are: the Mississippi Fan (MF, orange); the deep northeastern GoM (dNEG, solid blue); the deep eastern GoM (dEG, green); the deep southeastern GoM (dSEG, solid red); the deep central GoM (dCG, yellow); the Dry Tortugas (DT, magenta); the northern Campeche Bank (NCB, dashed red); the eastern Campeche Bank (ECB, dashed blue). Isobaths of 200 m, 2000 m, and 3000 m are plotted in thin black lines.

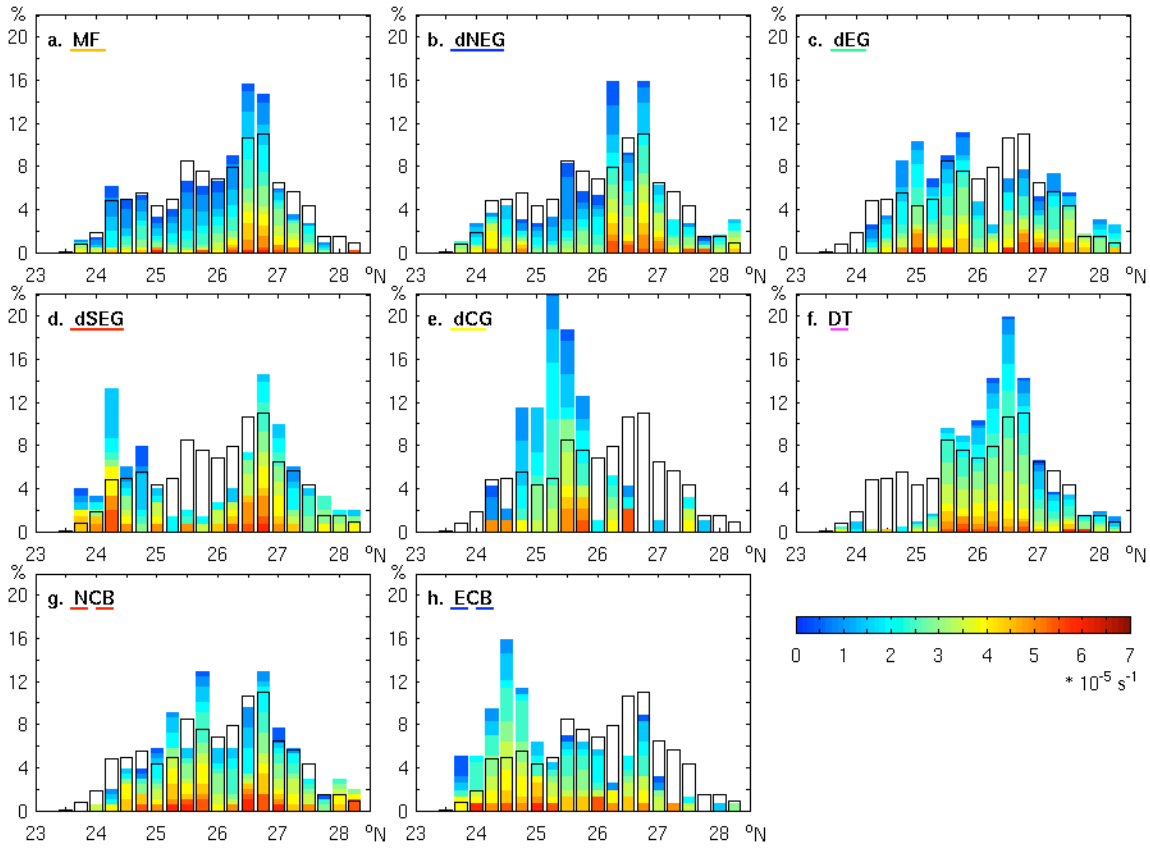

Figure 5. Normalized distribution of the LC northern extension at the time of cyclone detection (color-filled histograms, degrees of latitude, 23.0 – 28.5°N), for the eight regions of interest (see Figure 4). The LC northern extension is estimated from mapped AVISO SSH data (see text for more details). In color is the associated relative vorticity (10^{-5} s^{-1}). The reference distribution of the LC northern extension at all times is added in each subplot (histograms with thin black contours). Colors underlining each area name reference the colors used for that area in Figure 4.

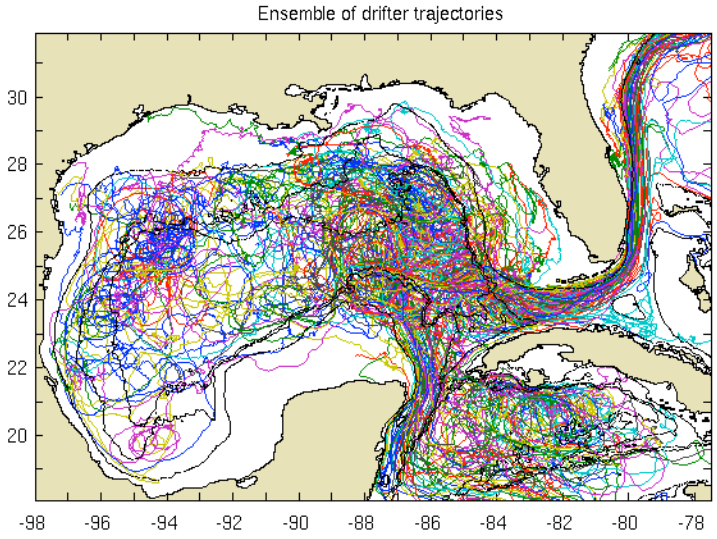

Figure 6. Trajectories of the 148 GDP drifters advected inside the GoM, from 1993 to 2011. Isobaths of 200 m, 2000 m, and 3000 m are plotted in thin black lines.

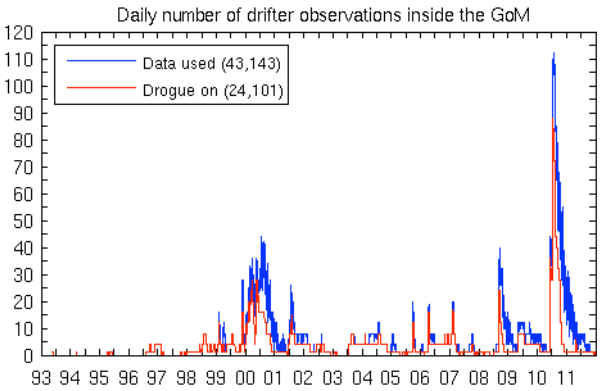

Figure 7. Time series of the daily number of drifter observations inside the GoM, for each year from 1993 to 2011 (x-axis). In red are the values when considering data only if the drifter's drogue is on; in blue are the values from the extended dataset (see Appendix B). The total number of observations in each case is indicated in the panel.

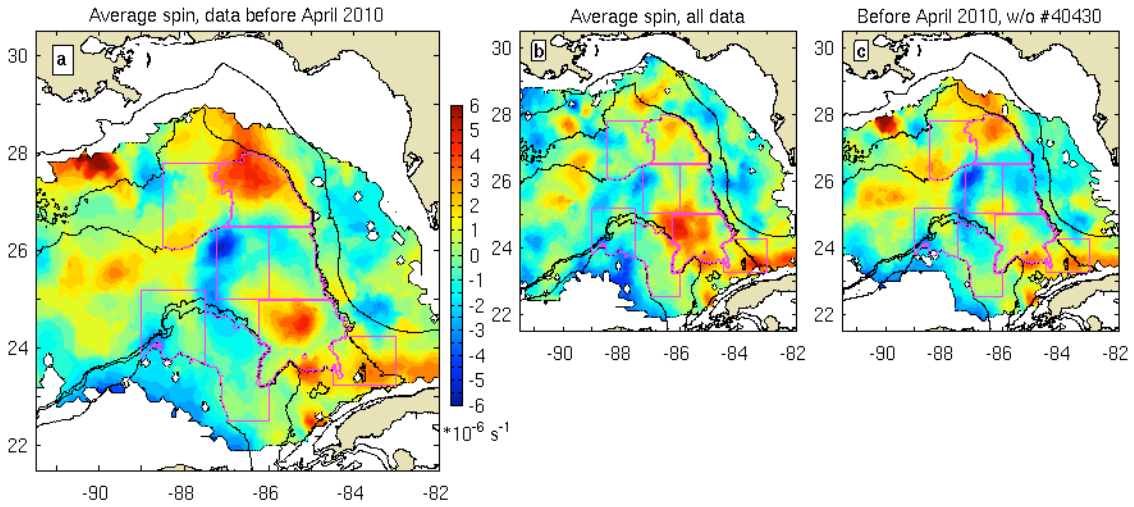

Figure 8. Average spin (Ω, 10^{-6} s^{-1}) estimated in the eastern GoM from the drifter trajectories. Patches of $\Omega>0$ denote cyclonic motion; patches with $\Omega<0$ denote anticyclonic motion. (a) All data before April 2010 are considered; (b) All data from 1993 to 2011 are considered; (c) All data before April 2010 are considered, with the exception of drifter #40430 (see Figure B1e).) Isobaths of 200 m, 2000 m, and 3000 m are plotted in thin black lines. The grid corresponding to various domains of interest defined in Figure 4 is added (thin magenta lines).

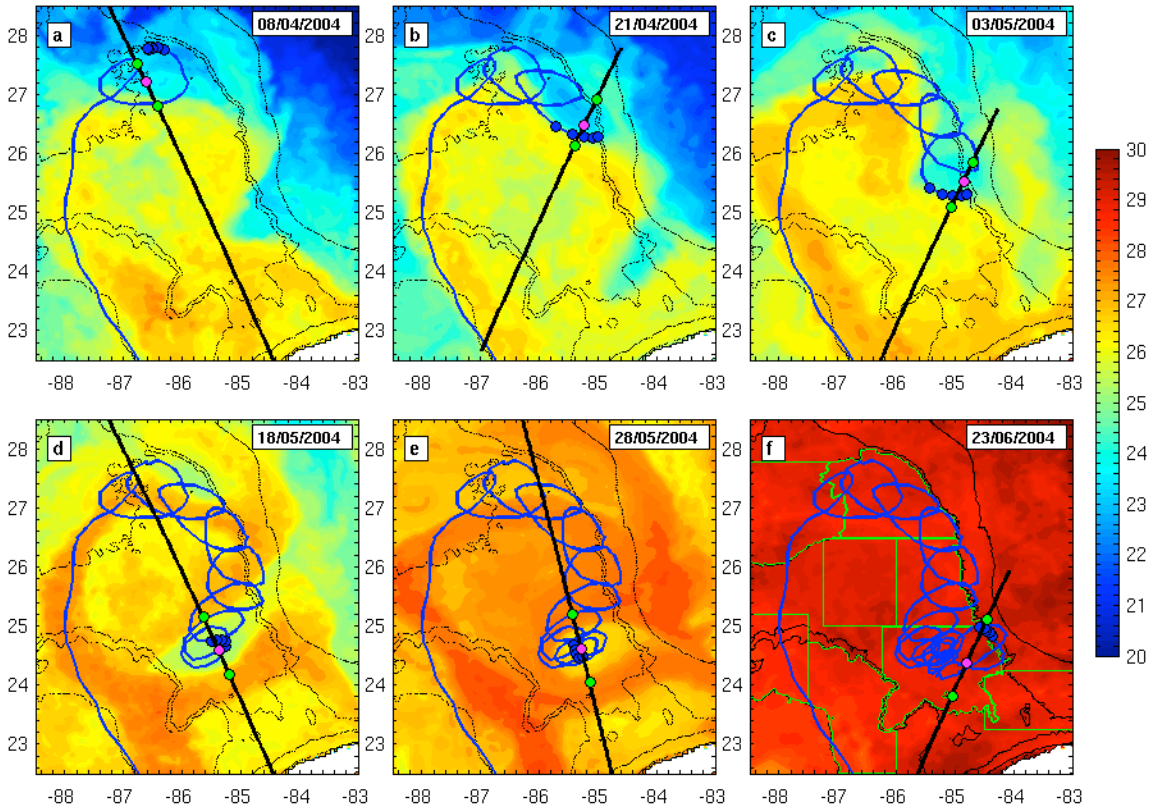

Figure 9. SST (°C) maps from the GHRSST-MUR dataset, with daily data at 0.011° resolution. The trajectory of drifter #40430 up to the SST observation date is depicted (blue line), with the locations of observations at the exact same date (blue points circled in black). The satellite track from one of the four altimeters in orbit, which detects a cyclone in the same area and same date (+/- 1 day) as the drifter looping, is added (thick black line), with the estimated center of the corresponding cyclone (magenta point circled in black), and the estimated cyclone boundaries (green points circled in black). The dates considered are: (a) April 8, 2004; (b) April 21, 2004; (c) May 3rd, 2004; (d) May 18, 2004; (e) May 28, 2004; (f) June 23, 2004. The grid corresponding to various domains of interest defined in Figure 4 is added (thin green lines). Isobaths of 200 m, 2000 m, and 3000 m are plotted in thin black lines.

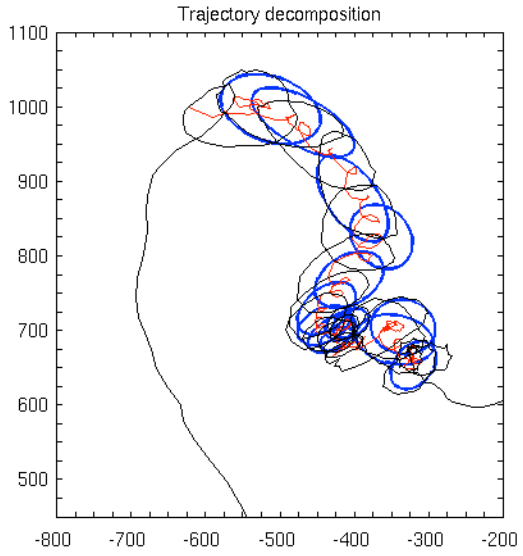

Figure 10. Decomposition of drifter #40430 trajectory in a geometric grid (km): reference trajectory (black), some of the ellipses estimated from the trajectory decomposition technique by Lilly et al. (2011, blue), residual (red).

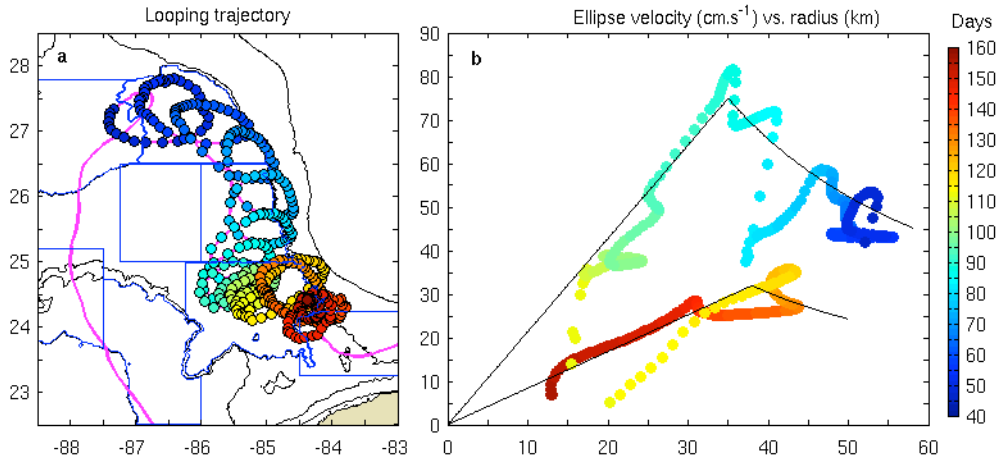

Figure 11. Focus on the elliptical part of the decomposition of drifter #40430 trajectory: (a) trajectory of the drifter (magenta line), with the locations and days (days since February 15, 2004) of individual observations corresponding to an elliptical motion as identified by the decomposition of the trajectory; the grid corresponding to various domains of interest defined in Figure 4 is added (thin blue lines); (b) Values of velocities (y-axis, $cm.s^{-1}$) vs. radius (x-axis, km), for each observation location shown in (a); (b) black lines denote estimated velocity profiles for Rankine-type cyclones approximately fitting the observed velocity-radius profiles (see text for more details).

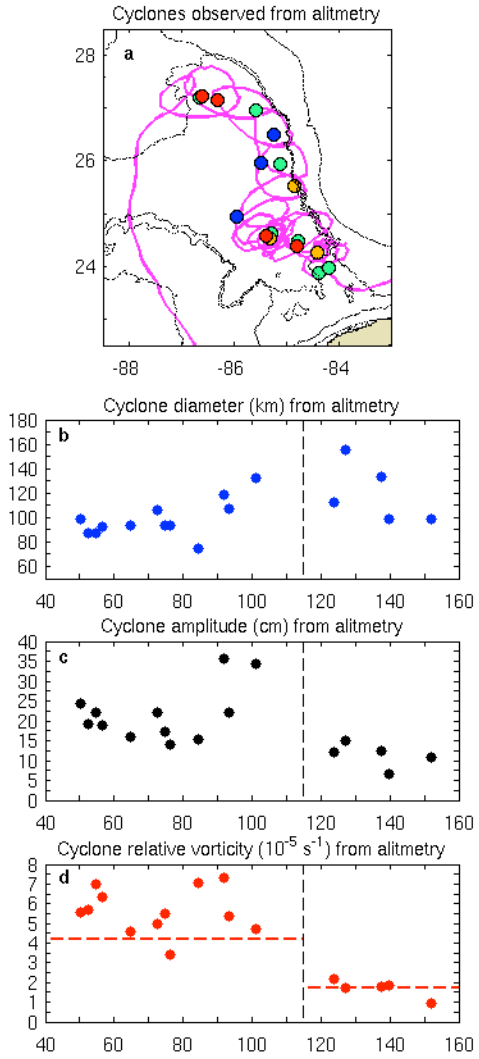

Figure 12. (a) Trajectory of drifter #40430 (magenta), with the individual altimetry observations of a cyclone at the location and date (+/- 1 day) of a drifter's loop (colored point circled in black, blue: Jason 1, red: Topex/Poseidon, green: Envisat, orange: GFO); (b) individual estimations of the cyclone diameter (km) from along-track altimetry, along the drifter trajectory (days since February 15, 2004); (c) same as (b), for the cyclone amplitude (cm); (d) same as (b) for the cyclone relative vorticity (10^{-5} s^{-1}); the two values estimated from the drifter trajectory decomposition are added for day 40 to day 115, and from day 115 to day 160, as a reference (dashed lines). (b-d) The collapse of the first eddy on day 115 (June 9, 2004) is added (vertical dashed black line).

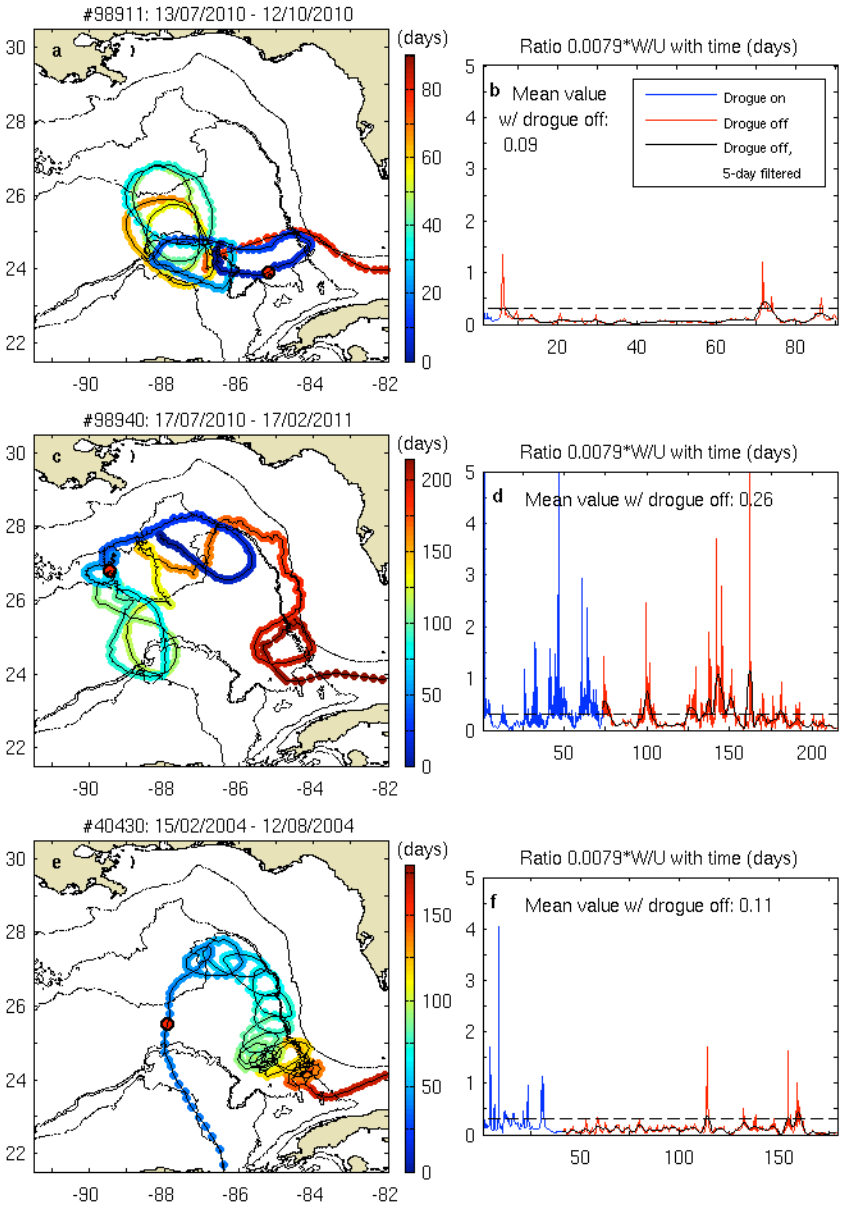

Figure B1. (a,c,e) Individual trajectories of three drifters, with associated age in the study area (in days). Each drifter identification number, initial and final dates in the area noted on Figure 6 are indicated in the title. Isobaths of 200 m, 2000 m, and 3000 m are plotted in thin black lines. (b,d,f) Time series (in days) of the ratio 0.0079*W/U, where W is the amplitude of the surface wind, and U the amplitude of the drifter velocity, for the three drifter trajectories; in blue is the period along the trajectory when the drifter's drogue is on, in red is the part when the drogue is off, and in black is the period when the drogue is off, low-pass filtered using a 5-day Loess filter; the mean value of the ratio for the period when the drogue is off is indicated in each panel; the value 0.3 is added on each panel (dashed black line), as a comparison.